Dalton Transactions

ROYAL SOCIETY OF CHEMISTRY

PAPER

View Article Online
View Journal | View Issue

Cite this: *Dalton Trans.*, 2024, **53**, 13871

Salicylaldehyde-derived piperazine-functionalized hydrazone ligand-based Pt(II) complexes: inhibition of EZH2-dependent tumorigenesis in pancreatic ductal adenocarcinoma, synergism with PARP inhibitors and enhanced apoptosis†

Zhimin Lv,‡[a] Amjad Ali,‡[b,c] Cheng Zou,[a] Zerui Wang,[a] Minglu Ma,[a] Na Cheng,[a] Man Shad,[a,d] Huifang Hao,[a,d] Yongmin Zhang *[a,e] and Faiz-Ur Rahman *[a]

Received 27th April 2024,
Accepted 16th July 2024

DOI: 10.1039/d4dt01243g

rsc.li/dalton

Piperazine is an important functional unit of many clinically approved drugs, including chemotherapeutic agents. In the current study, methyl piperazine was incorporated and eight salicylaldehyde-derived piperazine-functionalized hydrazone ONN-donor ligands (L) and their Pt(II) complexes (L-PtCl) were prepared. The structures of all these ligands (**L1–L8**) and Pt(II) complexes (**C1–C8**) were determined using ^{1}H and ^{13}C NMR, UV-vis, FT-IR and HR-ESI MS analyses, whereas the structures of **C1**, **C5**, **C6**, **C7** and **C8** were determined in the solid state using single crystal X-ray diffraction analysis. Solution state stabilities of **C3**, **C4**, **C5** and **C6** were determined *via* time-dependent UV-vis spectroscopy. All these complexes (**C1–C8**) were studied for their anticancer effect in pancreatic ductal adenocarcinoma cells, including BxPC3, MIAPaCa-2 and PANC1 cells. **C1–C8** displayed a potential cytotoxic effect in all these cancer cells, among which **C5**, **C6** and **C8** showed the strongest inhibitory effect in comparison with standard chemotherapeutic agents, including 5-fluorouracil (5-FU), cisplatin (CP), oxaliplatin and doxorubicin (DOX). **C5**, **C6** and **C8** suppressed the growth of pancreatic cancer cells in a dose-dependent manner. Moreover, **C5**, **C6** and **C8** inhibited clonogenic potential and invasion ability and induced apoptosis in PANC1 cells. Importantly, **C5**, **C6** and **C8** synergized the anticancer effect with PARP inhibitors, including olaparib, veliparib and niraparib, in pancreatic cancer cells, thus suggesting an important role of **C5**, **C6** and **C8** in induction of apoptosis in combination with PARP inhibitors. **C5** combined with PARP inhibitors induced caspase3/7 activity and suppressed ATP production. Mechanistically, **C5**, **C6** and **C8** inhibited EZH2 protein expression to suppress EZH2-dependent tumorigenesis. Overall, these results highlighted the importance of these piperazine-functionalized Pt(II) complexes as potential anticancer agents to suppress pancreatic ductal adenocarcinoma tumorigenesis by targeting the EZH2-dependent pathway.

Introduction

Cisplatin is a first-line chemotherapy drug approved for cancer treatment; similarly, other related platinum drugs have been approved, such as carboplatin and oxaliplatin.[1] When cisplatin or other related chemotherapeutic drugs enter tumor cells, their ancillary ligand(s) is(are) replaced by H_2O, thus activating platinum drugs and finally binding to the DNA guanine base through different linkages, including inter-/intra-strand cross-linking, which twists the DNA helix, further inhibits DNA transcription and finally causes tumor cell apoptosis.[2] Cisplatin, as a bifunctional platinum(II) complex, has been widely used, but it causes a variety of side effects and faces a certain degree of drug resistance in cancer patients. Several other platinum-based drugs were later reported to overcome certain issues faced by cisplatin therapy. Therefore, the search for other plati-

[a]*Inner Mongolia University Research Center for Glycochemistry of Characteristic Medicinal Resources, Department of Chemistry and Chemical Engineering, Inner Mongolia University, Hohhot, People's Republic of China.*
E-mail: Yongmin.zhang@upmc.fr, faiz@imu.edu.cn
[b]*Institute of Integrative Biosciences, CECOS University of IT and Emerging Sciences, Peshawar, KPK, Pakistan*
[c]*Institute of Biomedical Sciences, School of Life Sciences, East China Normal University, 500 Dongchuan Road, Shanghai, 200241, People's Republic of China*
[d]*School of Life Sciences, Inner Mongolia University, Hohhot 010021, People's Republic of China*
[e]*Sorbonne Université, CNRS, Institut Parisien de Chimie Moléculaire, UMR 8232, 4 Place Jussieu, 75005 Paris, France*

†Electronic supplementary information (ESI) available: Stability figures, ^{1}H, ^{13}C NMR and MS spectra. CCDC 2344817–2344821. For ESI and crystallographic data in CIF or other electronic format see DOI: https://doi.org/10.1039/d4dt01243g

‡These authors contributed equally to this work.

num drugs continues; recently, a new class of monofunctional platinum complexes has been developed.[3] Monofunctional platinum complexes can only form a single adduct with DNA (Fig. 1),[4] and the binding rate is significantly increased, thereby resulting in additional interaction and steric hindrance, reducing the transcriptional repair function of cells, causing more serious DNA damage and inducing apoptosis.[5] When a chlorine atom of cisplatin was replaced by a ligand with a larger steric hindrance, a higher biological activity was observed.[6] Based on this idea, larger-sized N-heterocycles have been widely studied as ligands in monofunctional platinum complexes.[7] Stephen J. Lippard and co-workers have studied a variety of monofunctional platinum complexes, such as pyriplatin and phenanthriplatin, which showed good antitumor activity.[8] Among them, phenanthriplatin is an important preclinical anticancer drug.[9] Since then, various N-heterocyclic ligands have been introduced into the synthesis of monofunctional platinum complexes, and the antitumor activity was observed higher than that of cisplatin.[10] N-heterocycle coordinated luminescent monofunctional Pt(II) complexes were prepared with photosensitizers, such as porphyrin and boron-dipyrromethene (BODIPY). These complexes showed synergistic chemotherapeutic and photodynamic therapeutic (PDT) effects and higher antitumor activity and overcame drug resistance.[11–14] To improve the antitumor efficacy of platinum complexes, targeted monofunctional platinum chemotherapeutic drugs with different anticancer mechanisms were developed by chemical modification of the coordination assemblies.[15–18] By changing the ligand or substituents on the ligand, a series of monofunctional platinum antitumor drugs were obtained, and all these complexes showed good antitumor activity in breast, lung, liver and other cancer cell lines.[19–23]

Hydrazones (R1CH = N-NR2R3) belong to the Schiff base family; many hydrazones have antitumor and other biological activities, and the presence of hydrazones functional group in a drug increases lipophilicity, thus resulting in increased drug absorption.[24–26] Benzophenone-based hydrazone derivatives were used as cathepsin inhibitors that inhibited the proliferation of A498 renal cancer cells.[27] Asulfonamide and pyridine are linked by hydrazone structure as VEGFR-2 inhibitors, which have good anti-proliferative activity against different types of cancer cells.[28–30] As a linker, the hydrazone group could hydrolyse in the acidic pH of the tumor environment; therefore, it can be used as a delivery carrier to specifically deliver drugs to tumor tissues.[31] As a multifunctional ligand, hydrazone is easy to coordinate with most metals to exert better antitumor activity, and various hydrazone-coordinated metal complexes have been prepared and studied for their antitumor activities, including complexes of Ni(II), Co(II), Zn(II), Cu(II), Cd(II), Mn(II), Ru(II) and Pt(II).[32–40]

Piperazine (1,4-diazocyclohexane) is an important drug scaffold that is often used to connect substructures with good biological activity and major N-heterocycles commonly used in small drug molecules. Piperazine functions in a drug could improve pharmacokinetic characteristics, such as enhancing target affinity and specificity and improving water solubility, oral bioavailability, ADME (absorption, distribution, metabolism and excretion) and other characteristics.[41,42] Piperazine and its derivatives have a wide range of biological activities, such as anticancer,[43] anti-viral,[44] antibacterial,[45] anti-glaucoma,[46] and anti-convulsion.[47] Approximately 100 drugs have been approved worldwide containing piperazine heterocyclic skeletons; among them, anticancer drugs are also included, such as avapritinib, gastrointestinal stromal tumors (GISTs), olaparib, ponatinib, and palbociclib.[48,49] As an important drug scaffold, piperazine derivatives were also combined with various natural antitumor drugs, such as artemisinin piperazine derivatives,[50,51] rhein piperazine,[52] and naringenin piperazine derivatives.[53] In addition, piperazine is used as a potential ligand in the synthesis of Pt-based anticancer complexes and is studied *in vitro* in different cancer cells.[54]

Pancreatic ductal adenocarcinoma (PDAC) is one of the most lethal types of human cancer; PDAC initial diagnosis is very challenging due to its metastasized nature, and it is very difficult to detect this disease at an early stage.[55] Around 75% of PDAC patients are mainly diagnosed when they suffer from stage 3 or stage 4 diseases. PDAC patients show the worst prognosis and poor survival rates. Due to its high metastatic nature, most of the PDAC patient's survival is less than 5 years.[56] Due to the complex nature of this disease, PDAC patient's treatment is also challenging. PDAC cells show high proliferation, migration, and invasion ability, finally leading to tumor burden in primary and secondary organs of the body.[57] PDAC is most often associated with epithelial–mesenchymal-transition (EMT) and cellular plasticity, which finally leads to therapy resistance. Therefore, most of the PDAC cells show resistance to chemotherapy, immunotherapy and radiotherapy.[58] The self-renewal capacity of pancreatic cancer stem cells also plays a major role in the recurrence of pancreatic cancer. Activation of oncogenic signalling pathways, such as KRAS, NF-κB, VEGF, MEK/MAPK/ERK kinases, PI3K-AKT-mTOR signalling pathway, c-MYC and TGF-β signalling, play important roles in the pancreatic cancer progression, chemo-resistance and metastasis.[59] Due to its complex and lethal nature, the

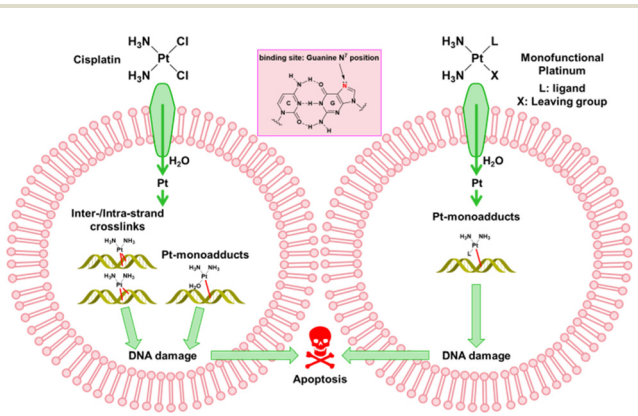

Fig. 1 Antitumor mechanism of cisplatin and monofunctional platinum complexes.

identification of novel chemotherapeutic agents is considered important for better treatment of PDAC patients.

Enhancers of zeste homolog 2 (EZH2) have been shown to play important roles in invasion, metastasis, migration and tumorigenesis.[60] EZH2 prolongs cancer cell survival by regulating cell cycle progression and plays an important role in the inhibition of apoptosis, thereby leading to tumor development. EZH2 overexpression has been shown in pancreatic, prostate, oesophageal, breast, gastric and nasopharyngeal cancers. High expression of EZH2 is associated with decreased survival and worst prognosis in cancer patients. Inhibition of EZH2 is associated with decreased invasion, migration and suppression of metastasis and EMT. EZH2 has been shown to promote cisplatin resistance by targeting c-MYC. EZH2 also promotes resistance to gefitinib by activating AKT/PI3K signalling pathway. Moreover, EZH2 plays an important role in tamoxifen resistance by targeting ERα-GREB1 signaling.[61] EZH2 has been shown to promote resistance to sunitinib in renal cell carcinoma by targeting the receptor tyrosine kinase (RTK) signalling pathway. EZH2 has been shown to increase the expression of multidrug resistance proteins (MRPs) and thus plays a critical role in drug resistance in different types of human cancers.[62] Inhibition or suppression of EZH2 increases the expressions of tumor suppressor genes, such as p15, p21, p27, PUMA and caspase 3/8 activation, and finally leads to apoptosis. Thus, EZH2 is considered an important target in the field of both translational and clinical cancer research, and several inhibitors have been developed, such as 3-deazaneplanocin A (DZNep), EPZ-005687, GSK926, and UNC-1999, to inhibit the expression of EZH2.[63] Therefore, the identification of novel chemotherapeutic agents to target EZH2 expression is considered important in the field of cancer therapy.

We have extensively studied the synthesis of novel functionalized salicylaldimine/hydrazone assembly-based metal complexes and their antitumor evaluation.[20–22,40] The above discussion of the previously reported literature and our experience in the related field prompted us to develop a new type of salicylaldehyde-derived piperidine-functionalized hydrazone-based ligands and a new class of monofunctional platinum complexes with Cl as an ancillary ligand for antitumor research. The structures and related stabilities of the ligands (**L1–L8**) and platinum complexes (**C1–C8**) were characterized by applying detailed analytical methods. The crystal structures of five complexes **C1**, **C5**, **C6**, **C7** and **C8** were determined by single crystal X-ray analysis. *In vitro* biological activity tests were performed in pancreatic ductal adenocarcinoma cells, including BxPC3, MIAPaCa-2 and PANC1 cells, using MTT assays. The results showed that these complexes could significantly inhibit cancer cell growth, cloning and migration of pancreatic ductal adenocarcinoma (PDAC) cells. The anticancer effects were compared with multiple anticancer drugs. These platinum complexes induced apoptosis by inhibiting EZH2-dependent tumorigenesis in PDAC and synergistically enhanced cell death when used in combination with PARP inhibitors (Olaparib, Veliparib and Niraparib).

Results

Chemistry

ONN-donor tridentate piperazine functionalized hydrazone ligands (**L1–L8**) were prepared by the reaction of substituted salicylaldehyde and 1-amino-4-methylpiperazine in ethanol at reflux. Monofunctional Pt(II) complexes (**C1–C8**) were prepared by reacting K_2PtCl_4, NaOAc and particular ligand in a 1.1 : 1.1 : 1 ratio in a refluxing DMSO/methanol mixture. All these ligands (**L1–L8**) and complexes (**C1–C8**) were obtained in excellent isolated yields (Scheme 1) and characterized by applying multiple analytical methods (ESI Fig. S1–S64†). The structures of **C1**, **C5**, **C6**, **C7** and **C8** were determined by single crystal X-ray analysis.

In the ^{1}H NMR spectra of **L1–L8** phenolic protons, a chemical shift was observed in the 11.11–12.90 ppm region; proton chemical shifts around 2.60–3.29 ppm were assigned to the piperazine ring's protons, and the chemical shift around 2.35–2.38 ppm was assigned to the methyl group at the N position of piperazine. Proton chemical shifts in the aromatic region (6.67–8.59 ppm) belonged to the proton chemical shifts of the aromatic ring, which were slightly different in each ligand due to different substituents on the salicylaldimine aromatic ring. The biggest difference between the ^{1}H NMR of **C1–C8** and **L1–L8** is the disappearance of the phenolic hydroxyl proton signals around 11–12.90 ppm region, showing the covalent bond formation between the ligand OH group and Pt. The imine (CH═N) proton peak of the hydrazone was found in the 8.88–9.65 ppm range for **C1–C8**, which moved significantly downfield compared to the particular free ligand (**L1–L8**). Similarly, slight changes were observed in the ^{13}C NMR spectra of **L1–L8** and **C1–C8**, and different carbon chemical shifts of the ligands shifted up or downfield slightly in the complexes.

The UV-vis spectral analyses of the ligands (**L1–L8**) and complexes (**C1–C8**) were performed in chloroform, and all the spectra were plotted in Fig. 2. Different changes in the absorption peaks of the ligands and complexes were observed in the UV-vis spectra plots (Fig. 2A and B). All the absorption peaks of the ligands were observed in the UV region below 400 nm. In the UV-vis, spectra of the complex absorption in the visible

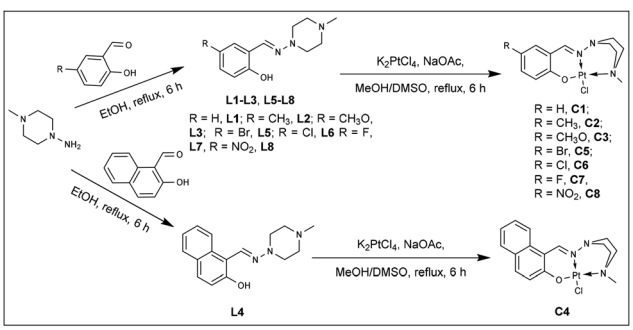

Scheme 1 Steps for the synthesis of ligands (**L1–L8**) and Pt(II) complexes (**C1–C8**).

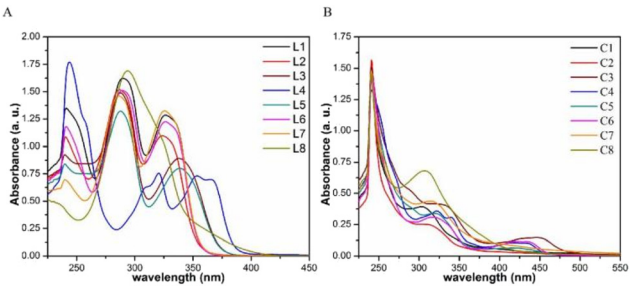

Fig. 2 UV-vis absorption spectra plot of **L1–L8** (A) and **C1–C8** (B).

region were also observed. The absorption peak near 250 nm is caused by ligand-to-ligand charge transfer (LLCT), and the absorption peak near 320–350 nm is caused by $\pi \rightarrow \pi^*$ transition between the C═N double bond and aromatic ring. In the case of **C4**, a slight difference observed in these transitions could be due to the presence of a naphthalene ring, which increased the aromaticity and planarity. The absorption peak for each complex in the range of 430–450 nm is caused by metal-to-ligand charge transfer (MLCT). For **C3**, this absorption peak is red shifted due to the presence of an electron rich methoxy group on the aromatic ring.

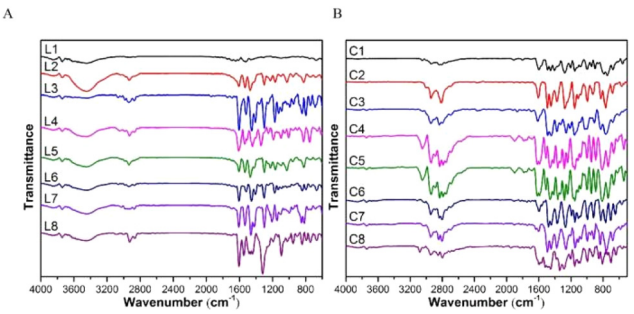

Fig. 3 FT-IR spectra plot of **L1–L8** (A) and **C1–C8** (B).

The FT-IR spectra of **L1–L8** and **C1–C8** were measured in the solid state by applying the KBr tableting method (Fig. 3 and ESI Fig. S49–S64†). The comparative plot clearly showed the phenolic O–H stretching frequency for **L1–L8** near 3400 cm^{-1}, the transmittance peak of C–H stretching frequency near 3200–2800 cm^{-1}, and the transmittance peak of C═N double bond stretching near 1600 cm^{-1} (Fig. 3A). Compared with Fig. 3A, it can be observed in Fig. 3B that the phenolic hydroxyl transmittance peak of **C1–C8** near 3400 cm^{-1} disappeared, showing the O–Pt bond formation in all these complexes. The other transmittance peaks of C–H stretching of the hydrogen of each ligand in each complex around 3200–2800 cm^{-1} and the C═N double bond transmittance peak near 1600 cm^{-1} also existed with a slight shift compared to the ligand.

Single crystal description of C1, C5, C6, C7 and C8

The single crystal of each complex (**C1**, **C5**, **C6**, **C7** and **C8**) was obtained by applying a slow solvent evaporation method using a clear solution in CH_2Cl_2/*n*-hexane (1 : 1) mixture. The crystal structure was determined by single-crystal X-ray diffraction. The detailed structural data are plotted in Fig. 4 (**C1**), 5 (**C5**), 6 (**C6**), 7 (**C7**) and 8 (**C8**), and the detailed crystal structure parameters are

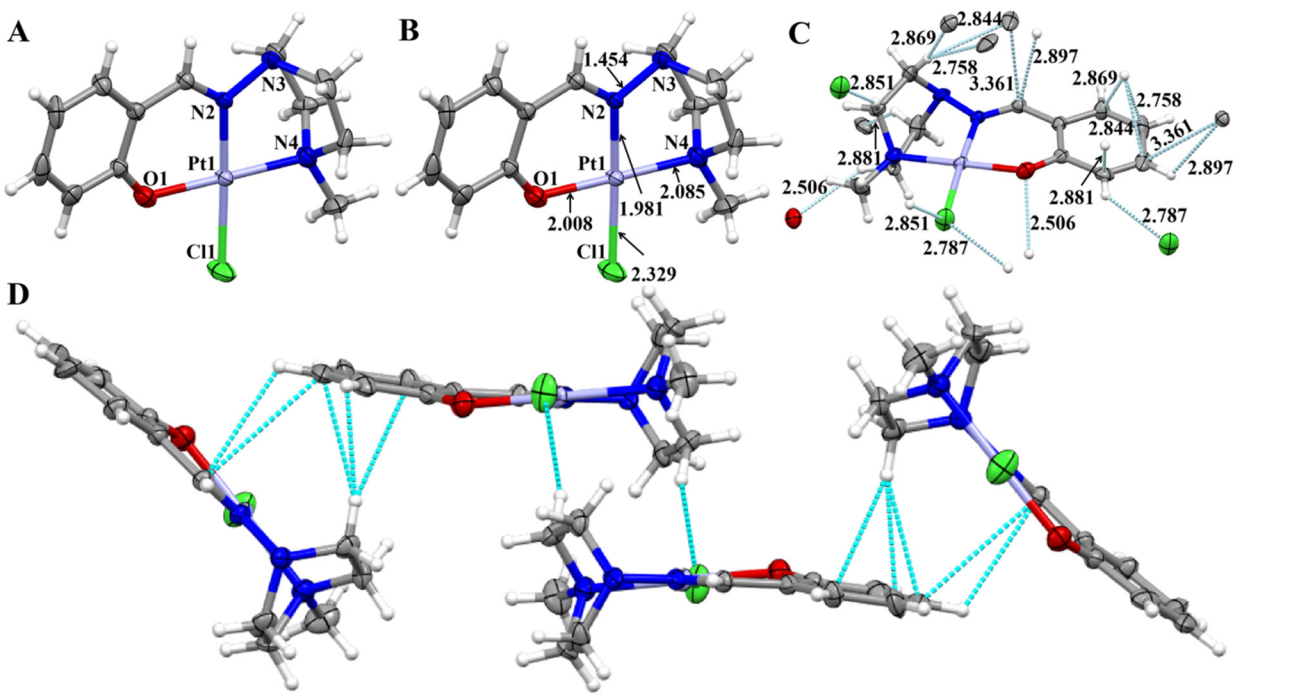

Fig. 4 Single crystal data plot of **C1** at 50% probability of thermal ellipsoids, showing atoms around the Pt(II) center (A), bond lengths (B), and close contacts (C) and (D) arrangement of molecules in crystal packing.

presented in Tables 1 and 2. **C1**, **C5**, **C6** and **C7** were crystallized in a monoclinic crystal system, while **C8** was crystallized in a triclinic crystal system. Pt atom symmetry was a square planner and bonded to ONN atoms of the main ligand and ancillary Cl (Fig. 4A, 5A, 6A, 7A and 8A).[64] The bond lengths (Fig. 4B, 5B, 6B, 7B and 8B) (Table 2 entries 1–4) and bond angles (Table 2 entries 5–10) of five platinum complexes **C1**, **C5**, **C6**, **C7** and **C8** were found to be almost similar. The longest bond at the Pt center in **C1**, **C5**, **C6**, **C7** and **C8** was Pt(1)–Cl(1/2). The shortest bond of Pt to other atoms in **C1**, **C5**, **C6** and **C7** was Pt(1)–N(1/2/3), while the shortest bond in **C8** was Pt(1)–N(3/4). The bond angle parameters of **C1**, **C5**, **C6**, **C7** and **C8** were similar; the largest bond angle was ∠O(1/3)–Pt(1)–N(3/4) in each complex, whereas the smallest bond angle was ∠O(1/3)–Pt(1)–Cl(1/2). The close interactions among molecules in crystal packing are shown in Fig. 4C, 5C, 6C, 7C, and 8C. The molecules of each complex were arranged in a three-dimensional space through these interactions in the crystal packing. The H atoms attached to the piperazine function of the ligand in each complex (**C1**, **C5**, **C6**, **C7** and **C8**) interacted with the C atoms of the salicylaldehyde aromatic ring in the crystal packing; similarly, the Cl atoms attached to Pt(II) strongly interacted with the neighbouring molecule hydrogens and formed a three-dimensional arrangement in the crystal packing (Fig. 4D, 5D, 6D, 7D, and 8D).

The biological activity of platinum complexes depends on their stability or uniformity under different biological conditions, solvents or the presence of water in the solution. In general, the solution of a platinum complex is prepared in DMSO or in combination with water or biological medium for the preliminary *in vitro* biological activity test. Therefore, it is important to analyze the stability in DMSO or water or their combination. Based on the mechanism of action of a platinum complex in cancer cells, it first forms H_2O-Pt(II) hydrate by removal of the labile/ancillary ligand-like chloride in **C1–C8** and interacts with a certain biomolecule of DNA to exert antitumor activity.[2] These two points are considered in developing platinum-based anticancer complexes to meet the minimum requirements of their antitumor applications. To check the stability in the solution state, we selected **C3**, **C4**, **C5** and **C6** as the reference complexes and performed repeated time-dependent analyses by UV-vis absorption spectroscopy in H_2O : DMSO or PBS (pH = 7.2) : DMSO, 1 : 1 mixture (ESI Fig. S65–S72†). The test results showed that the UV-vis absorption spectra of **C3**, **C4**, and **C5** remained the same during these repeated analyses for 7 days, showing that these complexes have good stability in the solution state in the DMSO/water mixture. The same mixture was used in the solution preparation for the biological analyses.

Table 1 Structure refinement parameters of **C1**, **C5**, **C6**, **C7** and **C8**

	C1	**C5**	**C6**	**C7**	**C8**
Empirical formula	$C_{12}H_{16}ClN_3OPt$	$C_{12}H_{15}BrClN_3OPt$	$C_{12}H_{15}Cl_2N_3OPt$	$C_{12}H_{15}ClFN_3OPt$	$C_{12}H_{15}ClN_4O_3Pt$
Formula weight	448.82	527.72	483.26	466.81	493.82
Temperature (K)	149.99(10)	149.99(10)	150.00(10)	149.99(10)	150.00(10)
Crystal system	Monoclinic	Monoclinic	Monoclinic	Monoclinic	Triclinic
Space group	$P2_1/n$	$P2_1/n$	$P2_1/n$	$P2_1/n$	$P\bar{1}$
Unit cell dimensions					
a (Å)	10.0851(11)	11.0059(6)	10.8638(5)	10.2897(5)	7.9549(8)
b (Å)	10.6903(9)	11.2147(6)	11.1381(4)	10.8250(4)	9.4351(10)
c (Å)	12.4850(9)	11.9096(6)	11.8396(5)	12.0729(5)	10.4761(10)
α (°)	90	90	90	90	84.970(8)
β (°)	103.388(8)	105.554(5)	105.065(5)	102.743(4)	69.813(9)
γ (°)	90	90	90	90	72.252(9)
Volume (Å^3)	1309.5(2)	1416.14(13)	1383.38(10)	1311.62(10)	702.73(13)
Z	4	4	4	4	2
Density (calculated) (mg m^{-3})	2.277	2.475	2.320	2.364	2.334
Absorption coefficient (mm^{-1})	10.911	12.913	10.523	10.908	10.189
F(000)	848.0	984.0	912.0	880.0	468.0
Crystal size (mm^3)	0.12 × 0.1 × 0.09	0.12 × 0.09 × 0.06	0.12 × 0.1 × 0.08	0.11 × 0.09 × 0.08	0.12 × 0.11 × 0.09
Theta range for data collection (°)	4.694 to 49.994	4.478 to 49.998	4.536 to 50	4.716 to 49.992	4.144 to 49.998
Index ranges	$-8 \le h \le 11$, $-12 \le k \le 12$, $-14 \le l \le 13$	$-13 \le h \le 12$, $-13 \le k \le 11$, $-14 \le l \le 12$	$-12 \le h \le 10$, $-11 \le k \le 13$, $-14 \le l \le 14$	$-8 \le h \le 12$, $-9 \le k \le 12$, $-14 \le l \le 14$	$-9 \le h \le 9$, $-11 \le k \le 10$, $-10 \le l \le 12$
Reflections collected	5756	6286	5335	6059	4546
Independent reflections	2300 R_{int} = 0.0542, R_{sigma} = 0.0793	2502 R_{int} = 0.0363, R_{sigma} = 0.0464	2429 R_{int} = 0.0280, R_{sigma} = 0.0420	2319 R_{int} = 0.0315, R_{sigma} = 0.0409	2483 R_{int} = 0.0354, R_{sigma} = 0.0587
Data/restraints/parameters	2300/46/164	2502/0/173	2429/0/173	2319/12/173	2483/0/191
Goodness-of-fit on F^2	1.049	1.027	1.042	1.017	1.023
Final R indices $I > 2\text{sigma}(I)$	R_1 = 0.0367, wR_2 = 0.0585	R_1 = 0.0266, wR_2 = 0.0536	R_1 = 0.0236, wR_2 = 0.0406	R_1 = 0.0221, wR_2 = 0.0392	R_1 = 0.0279, wR_2 = 0.0502
R indices (all data)	R_1[a] = 0.0514, wR_2[b] = 0.0675	R_1[a] = 0.0329, wR_2[b] = 0.0566	R_1[a] = 0.0288, wR_2[b] = 0.0431	R_1[a] = 0.0268, wR_2[b] = 0.0412	R_1[a] = 0.0316, wR_2[b] = 0.0527
Largest diff. peak and hole (e Å^{-3})	0.98/−0.97	1.30/−1.12	0.87/−0.85	0.82/−0.73	0.91/−0.88

[a] $R_1 = \sum_{\text{all reflections}} |F_o - F_c| / \sum_{\text{all reflections}} |F_o|$. [b] $wR_2 = [\sum w(F_o^2 - F_c^2)^2 / \sum (w(F_o^2)^2)]^{1/2}$.

Table 2 Selected bond lengths (Å) and angles (°) around the Pt atom in each complex (**C1**, **C5–C8**)

Entry	Bond/angle	C1	C5	C6	C7	C8
Bond length (Å)						
1	Pt(1)–Cl(1/2)	2.3289(19)	2.3264(13)	2.3231(10)	2.3184(11)	2.3088(13)
2	Pt(1)–O(1/3)	2.009(6)	1.996(4)	1.997(3)	2.003(3)	1.997(4)
3	Pt(1)–N(1/2/3)	1.981(6)	1.965(4)	1.967(3)	1.963(4)	2.060(5)
4	Pt(1)–N(3/4)	2.086(7)	2.070(5)	2.070(4)	2.083(3)	1.963(4)
Bond angle (°)						
5	∠O(1/3)–Pt(1)–Cl(1/2)	85.09(15)	84.95(10)	84.96(8)	84.75(9)	84.38(10)
6	∠O(1/3)–Pt(1)–N(3/4)	178.8(2)	178.47(16)	179.02(13)	179.33(13)	177.80(14)
7	∠N(1/2/3)–Pt(1)–Cl(1/2)	176.7(2)	174.63(14)	174.45(11)	174.54(11)	95.93(12)
8	∠N(1/2/4)–Pt(1)–O(1/3)	92.3(2)	92.77(16)	93.01(13)	93.06(12)	93.05(17)
9	∠N(1/2/4)–Pt(1)–N(3/4)	86.9(3)	86.09(17)	86.21(14)	86.44(14)	86.68(18)
10	∠N(3/4)–Pt(1)–Cl(1/2)	95.72(18)	96.26(12)	95.87(9)	95.71(10)	177.25(14)

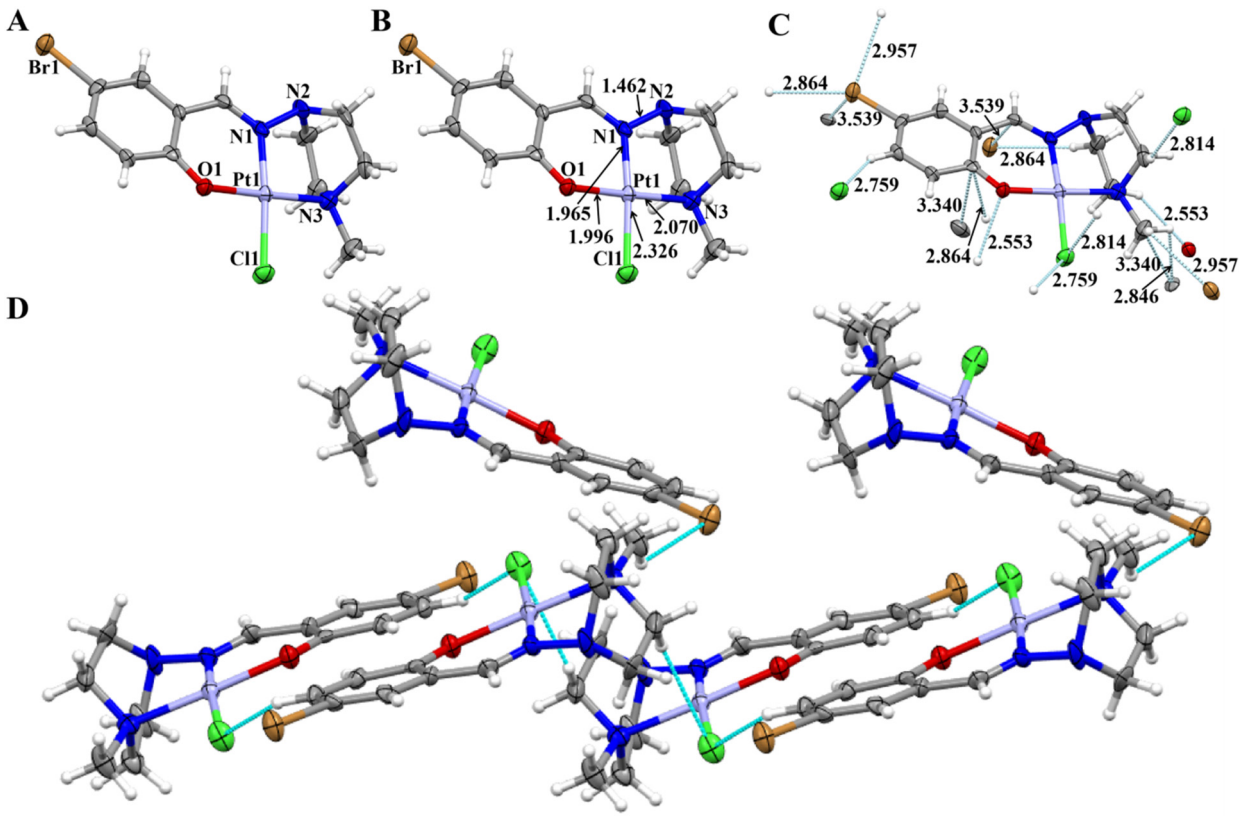

Fig. 5 Single crystal data plot of **C5** at 50% probability of thermal ellipsoids, showing atoms around Pt(II) center (A), bond lengths (B), close contacts (C), and arrangement of molecules (D) in the crystal packing.

Biology

Pancreatic ductal adenocarcinoma (PDAC) is a highly lethal malignant tumor, and chemotherapy is still the first-line treatment.[65] The cytotoxicity of the synthesized platinum complexes **C1–C8** was determined in PDAC cell lines, including BxPC3, MIAPaCa-2 and PANC1 cells. Cancer cells were treated with **C1–C8** (20 μM) for 48 h (Fig. 9A–C) and analysed by MTT assays. It can be observed that compared with the control group, the survival of PDAC cells treated with **C1–C8** was significantly decreased, which proved that this series of complexes could inhibit the survival of PDAC cells and had good cytotoxicity. A comprehensive evaluation of the data revealed **C5**, **C6** and **C8** as the three key complexes with good cytotoxicity in the whole series of **C1–C8**. Therefore, we tested the dose-dependent cytotoxicity assay of **C5**, **C6** and **C8** in these PDAC cells. BxPC3, MIAPaCa-2 and PANC1 cells were treated with 1.25, 2.5, 5, 10, 15 or 20 μM of **C5**, **C6** and **C8** for 48 h, respectively (Fig. 9D–F). The results showed that the survival rates of BxPC3, MIAPaCa-2 and PANC1 cells gradually decreased with the increase in the particular complex concentration. Compared with the control group, 1.25 μM of **C5**, **C6**

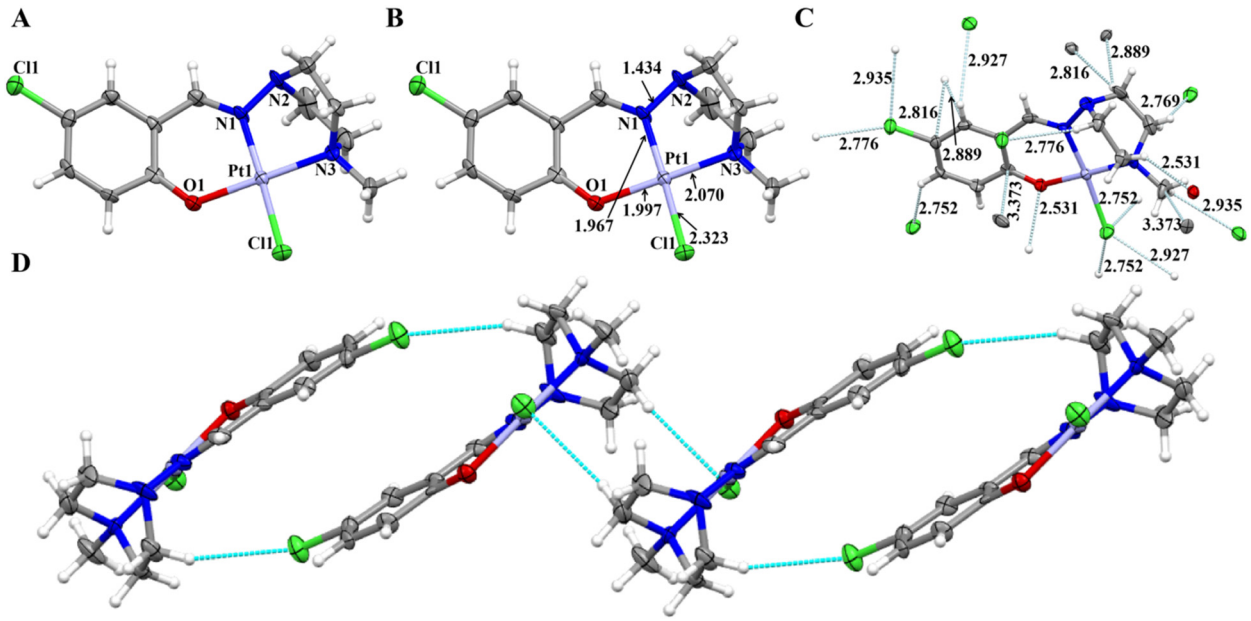

Fig. 6 Single crystal data plot of **C6** at 50% probability of thermal ellipsoids, showing atoms around Pt(II) center (A), bond lengths (B), close contacts (C), and arrangement of molecules (D) in crystal packing.

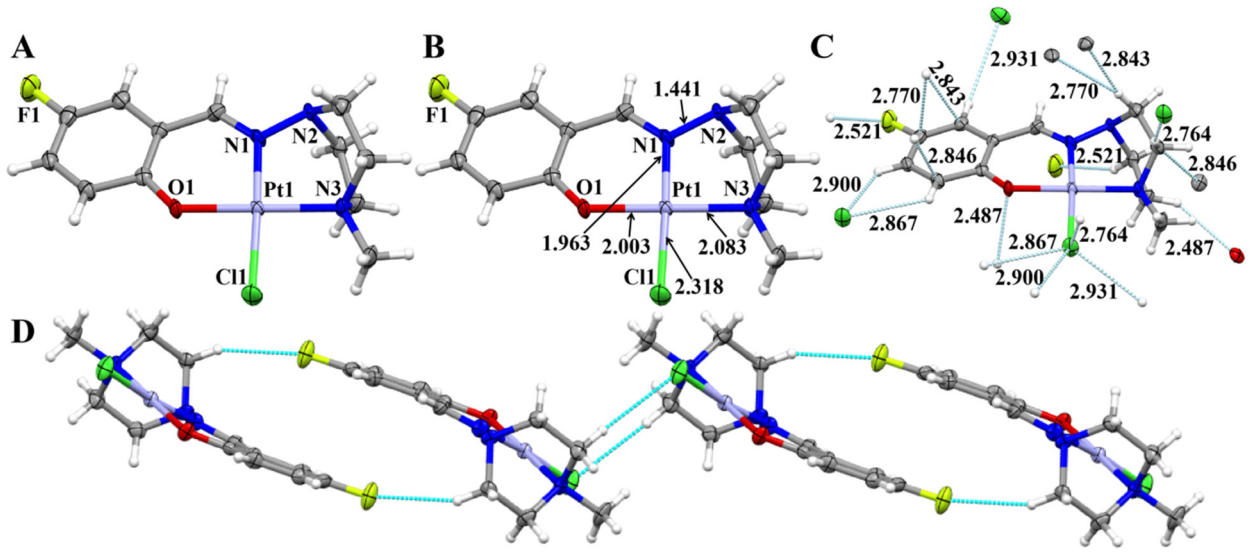

Fig. 7 Single crystal data plot of **C7** at 50% probability of thermal ellipsoids, showing atoms around Pt(II) center (A), bond lengths (B), close contacts (C), and arrangement of molecules (D) in crystal packing.

and **C8** inhibited the survival of BxPC3, MIAPaCa-2 and PANC1 cells, and 10 μM of **C5**, **C6** and **C8** was sufficient to inhibit the survival of BxPC3, MIAPaCa-2 and PANC1 cells, respectively. In summary, **C5**, **C6** and **C8** showed strong cytotoxicity in BxPC3, MIAPaCa-2 and PANC1 cells in a dose-dependent manner, respectively. These complexes inhibited the survival and proliferation of cancer cells. The anti-proliferative activity of the three highly active complexes (**C5**, **C6** and **C8**) could be arranged in series as follows: **C6** > **C5** > **C8**. Similarly, we used **C5**, **C6** and **C8** in normal cells 3T3 (mouse embryonic fibroblasts). We selected different concentrations of **C5**, **C6** and **C8** to detect the cytotoxicity of 3T3 cells (Fig. 10A–C). The increase in the concentration of each **C5**, **C6** and **C8** showed no obvious cytotoxicity to 3T3 cells, which suggested that these complexes are more active in cancer cells.

We compared the cytotoxicity of **C5**, **C6** and **C8** against BxPC3, MIAPaCa-2 and PANC1 cells with classical chemotherapeutic drugs cisplatin (CP), 5-fluorouracil (5-FU), oxaliplatin (OXA) and doxorubicin (DOX).[66] BxPC3, MIAPaCa-2 and PANC1 cells were treated with 10 μM of **C5**, **C6**, **C8**, CP, 5-FU,

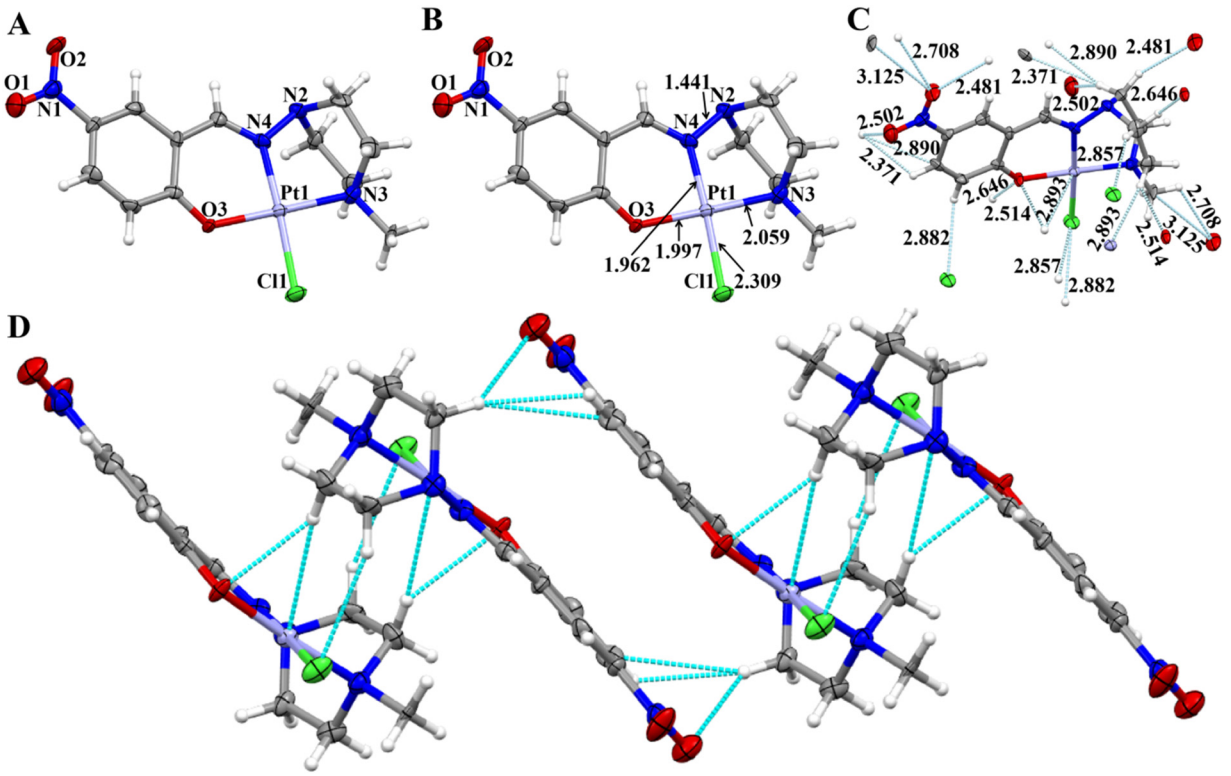

Fig. 8 Single crystal data plot of **C8** at 50% probability of the thermal ellipsoids, showing atoms around Pt(II) center (A), bond lengths (B), close contacts (C), and arrangement of molecules (D) in crystal packing.

OXA or DOX for 48 h (Fig. 11A–C). According to the MTT test results, **C5**, **C6**, and **C8** showed better cytotoxicity compared to the chemotherapeutic drugs cisplatin, 5-fluorouracil, oxaliplatin, and doxorubicin. The IC_{50} values for **C5**, **C6**, **C8**, CP, 5-FU, OXA or DOX were calculated in different cancer cells, as presented in Table 3. The survival rate of cancer cells treated with **C5**, **C6**, and **C8** was significantly lower, showing that these complexes effectively inhibited the growth and proliferation of BxPC3, MIAPaCa-2, and PANC1 cells.

The cloning of tumor cells can trigger their resistance to chemotherapeutic drugs, thereby promoting the survival, invasion and metastasis of tumor cells and increasing the difficulty of treatment.[67] Therefore, we tested the effects of **C5**, **C6** and **C8** on the colony formation ability of PANC1 cell (Fig. 12A–D). PANC1 cells were treated with 5 and 10 μM of **C5**, **C6** and **C8** for 7 days and analyzed by crystal violet assays. The results showed that **C5**, **C6** and **C8** suppressed the clonogenic potential of PANC1 cells in a dose-dependent manner. The inhibitory ability of the three complexes on the colony formation potential of PANC1 cells was compared as follows: **C6** > **C5** > **C8**. Next, we also observed the morphological changes in PANC1 cells upon treatment of **C5**, **C6** and **C8**. Interestingly, we detected apoptotic cells when PANC1 cells were treated with **C5**, **C6** and **C8** in a dose-dependent manner (Fig. 12E). These results indicated the strong inhibition of the tumorigenic potential and induction of the apoptosis of pancreatic cancer cells induced by these complexes.

Invasion of pancreatic cancer cells in the presence of C5, C6 and C8

The invasion of tumor cells results in the metastasis of tumor cells and promotes the development of cancer.[68] Therefore, suppression of the invasion of cancer cells inhibits cancer cell metastasis and further controls the development of cancer. To determine the ability of **C5**, **C6** and **C8**, we treated PANC1 cells with 10 μM of **C5**, **C6** or **C8** for 48 h, and cancer cell invasion was analyzed by invasion chambers (Fig. 13A–C). The results showed that the invasion ability of PANC1 cells treated with 10 μM of **C5**, **C6** and **C8** was significantly reduced. These results suggested that **C5**, **C6** and **C8** inhibited the invasion of PANC1 cells, thereby inhibiting metastasis and further decreasing the development of pancreatic cancer progression. The comparison of the three complexes inhibiting the invasion ability of PANC1 cells was listed as follows: **C6** > **C5** > **C8**.

DNA damage repair pathway depends on poly(ADP-ribose) polymerase (PARP); (PARP) inhibitors (PARPi) are a class of antitumor drugs that blocks DNA repair and induces the apoptosis of cancer cells by enzymatically inhibiting PARP activity at the site of DNA damage.[69] Olaparib, veliparib and niraparib are three widely used PARP inhibitors.[70–72] We used **C5**, **C6** and **C8** in combination with olaparib, veliparib and niraparib to explore their synergistic effect in PANC1 cancer cells (Fig. 14A–I). MTT data showed that compared with the control group, the viability of PANC1 cells treated with **C5**, **C6**, **C8**, ola-

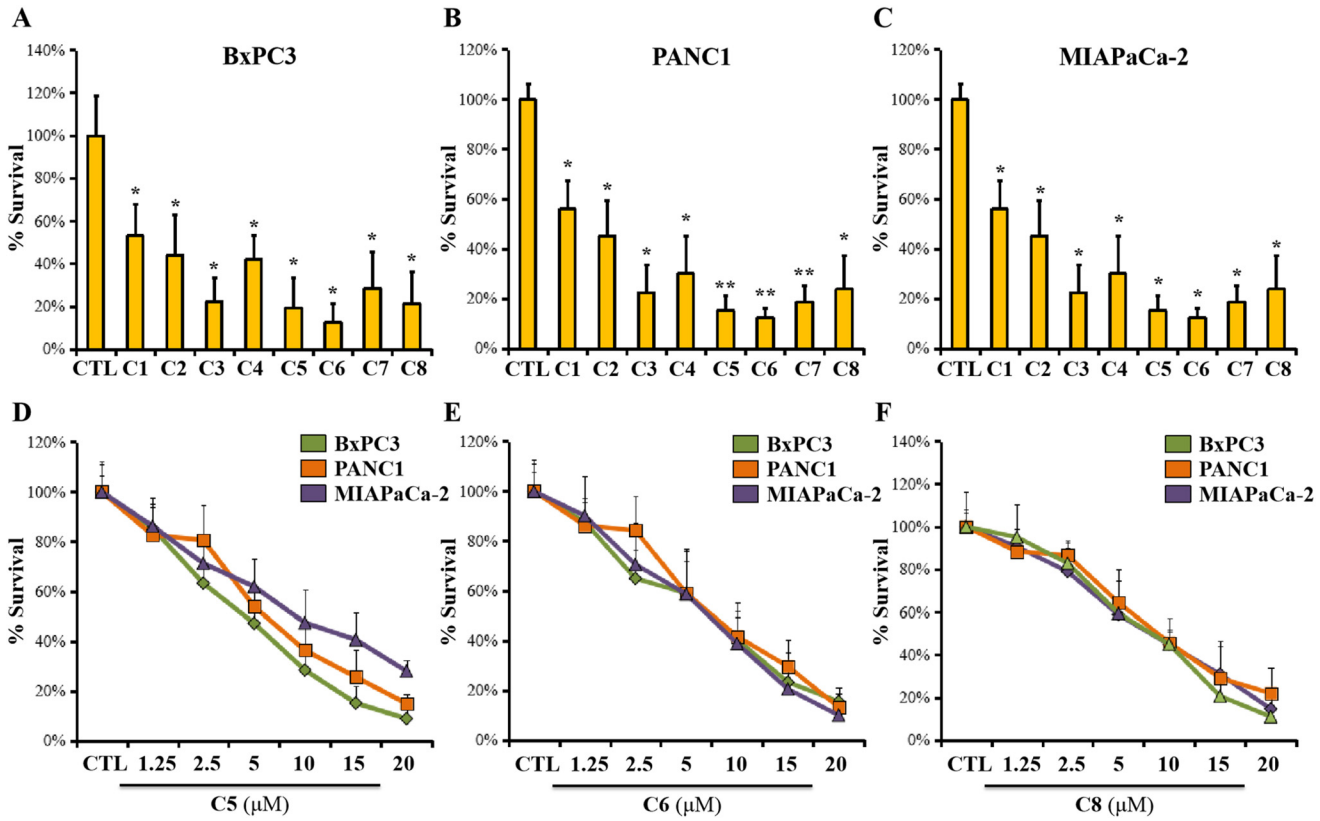

Fig. 9 **C1–C8** suppressed the proliferation of pancreatic cancer cells; (A–C) BxPC3, MIAPaCa-2 and PANC1 cells were treated with 20 μM of **C1–C8** for 48 h and cell viability was determined in percentage. (D–F) BxPC3, MIAPaCa-2 and PANC1 cells were treated with CTL, 1.25, 2.5, 5, 10, 15 or 20 μM of **C5**, **C6** or **C8** for 48 h, and cell viability was determined in percentage (CTL represents DMSO treatment). Statistical analysis represents the student *t*-test; **p* < 0.05; ***p* < 0.005.

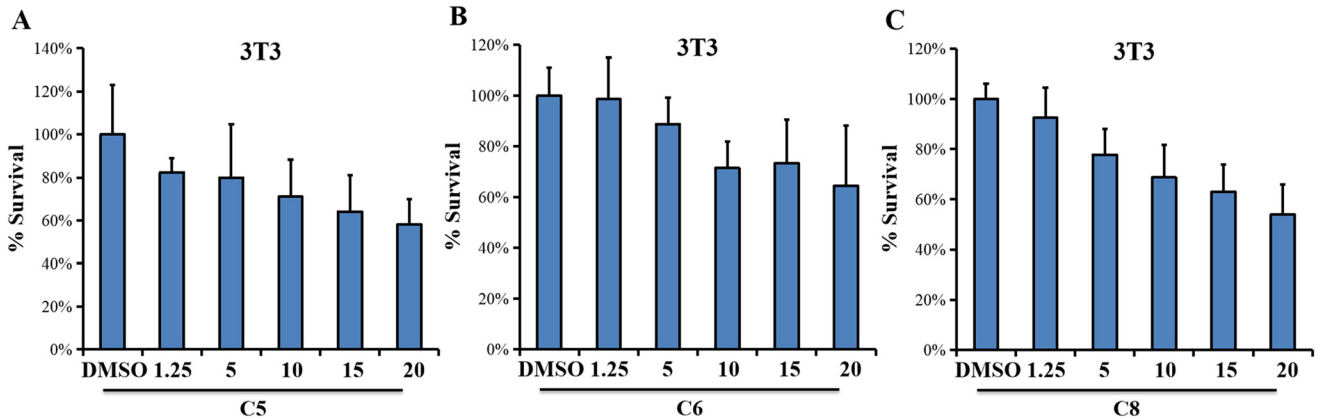

Fig. 10 **C5**, **C6** and **C8** have no obvious cytotoxicity towards 3T3 cells; (A–C) 3T3 cells were treated with DMSO and 1.25, 5, 10, 15 or 20 μM of **C5**, **C6** or **C8** for 48 h, and cell viability was determined.

parib, veliparib and niraparib alone was significantly reduced, but when **C5**, **C6** and **C8** were used in combinations, the survival rate of PANC1 cells was further reduced. Importantly, the **C5** and olaparib combination displayed a better combination index (CI = 0.713) in comparison to **C6** and olaparib (CI = 0.907); and **C8** and olaparib (CI = 1.225) combinations (Fig. 14A–C). Moreover, veliparib and **C6** combination (CI = 0.594) showed much stronger synergism when compared with **C5** and veliparib (CI = 0.751) combination and **C8** and veliparib (CI = 1.154) combination (Fig. 14D–F). Next, the niraparib and **C5** combination (CI = 0.751) showed a better combination index in comparison to niraparib and **C5** (CI = 0.786); niraparib and **C8** (CI = 0.863) combinations (Fig. 14G–I). Taken together, these results suggest that **C5**, **C6** and **C8** can

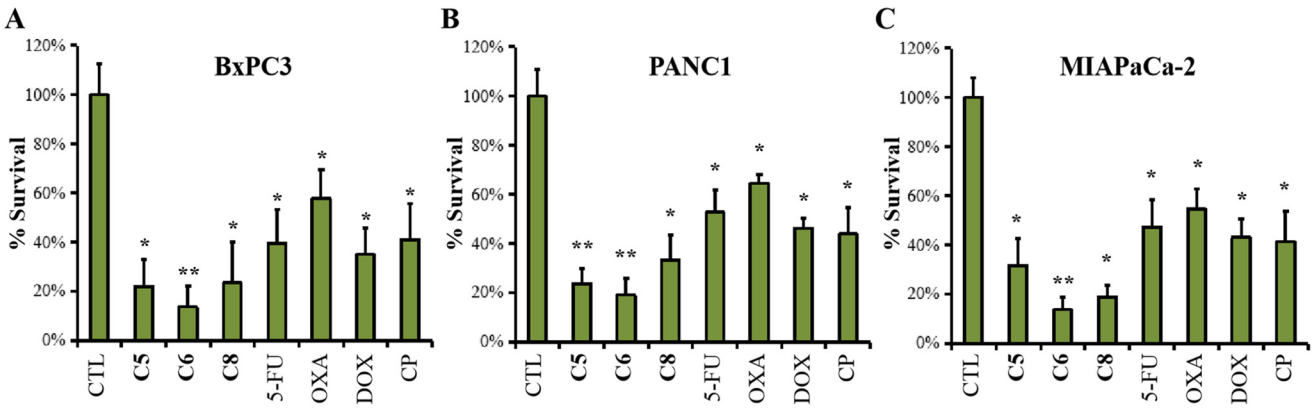

Fig. 11 Comparison of anticancer effects of **C5**, **C6** and **C8** with anticancer drugs; (A–C) BxPC3, MIAPaCa-2, and PANC1 cells were treated with 10 μM of **C5**, **C6**, **C8**, CP, 5-FU, OXA or DOX for 48 h, and cell viability was determined in percentage. CTL represents DMSO-treated cells. Statistical analysis represents the student *t*-test; $*p < 0.05$; $**p < 0.005$.

Table 3 IC_{50} (μM) values of **C5**, **C6**, **C8**, CP, 5-FU, OXA and DOX in different human cancer cells calculated from MTT data

	Complex			Market available anticancer drugs			
PDAC cell line	**C5**	**C6**	**C8**	CP	5-FU	OXA	DOX
BxPC3	5.47	7.32	8.23	9.76	9.89	14.54	10.88
PANC1	6.91	6.95	7.52	10.98	12.34	15.52	12.23
MIAPaCa-2	7.92	6.21	6.54	11.43	11.23	13.91	13.45

IC_{50} is defined as the concentration of a cytotoxic agent that is required for 50% inhibition of cell growth.

synergize the anticancer effect when used in combination with PARP inhibitors.

ATP (adenosine triphosphate), PARP and caspase-3/7 (pro-apoptotic factor) are closely related to cancer cell apoptosis. When PARP is inhibited, it leads to a severe DNA damage in tumor cells without repair; then, the expression of pro-apoptotic factor caspase-3/7 is activated, while PARP, as the substrate of caspase-3/7, is cleaved by caspase-3/7.[73,74] Consequently, PARP repair DNA requires continuous production of ATP to provide energy.[75,76] When PARP expression is inhibited or cleaved by caspase-3/7, intracellular ATP is not excessively consumed. PANC1 cells were treated with **C5** alone or in combination with olaparib, veliparib and niraparib caspase-3/7, and ATP assays were performed (Fig. 15A–F). We observed a significant increase in caspase-3/7 activity when **C5** was combined with olaparib, veliparib and niraparib (Fig. 15A–C). These results suggested that these drug combinations induced apoptosis in pancreatic cancer cells. Next, the combination of **C5** with olaparib, veliparib and niraparib further reduced the ATP production of PANC1 cells (Fig. 15D–F). These combinations reduced ATP production, thereby enhancing cell death and suppressing the tumorigenic ability of pancreatic cancer cells.

EZH2 (homolog 2) is a methylated histone transferase that is highly expressed in various tumor tissues and is closely related to the occurrence, development, invasion and metastasis of tumors.[77] EZH2 inhibits genes that lead to cell cycle arrest and promote self-renewal of tumor cells.[78] PANC1 cells were treated with 10 μM of **C5**, **C6** and **C8**, and the relative level of EZH2 protein was detected by western blot (Fig. 16A–F). The results showed that **C5**, **C6** and **C8** effectively inhibited the expression of EZH2 protein, thereby inhibiting the proliferation, invasion and metastasis of PANC1 cells.

Discussion

As a common drug in chemotherapy, the clinical application of platinum-based drugs (cisplatin, oxaliplatin, *etc.*) is limited by serious drug resistance and various adverse conditions in cancer patients.[79] In this context, monofunctional platinum complexes were investigated; based on the interaction and steric hindrance of the additional ligands, these complexes showed a higher anticancer rate and efficiency of binding to DNA to produce monoadducts, which reduced systemic side effects and improved drug resistance caused by the use of cisplatin.[20–23] As an important drug function and connection bridge, the hydrazone group has improved the lipophilicity of drugs and increased the absorption rate of drugs; many hydrazone derivatives have exhibited good antitumor activity.[24,27] As an important drug scaffold, piperazine positively affected the pharmacokinetic properties of drugs and improved the activities of drugs in many aspects. Similarly, various piperazine derivatives also showed good antitumor activities.[39–53] Based on the above background, we simply and efficiently synthesized a series of salicylaldehyde-derived piperazine functionalized hydrazone ligand-based platinum complexes **C1–C8** and performed their structural characterization and stability analyses using different analytical methods. The *in vitro* antitumor activity results showed that these complexes (**C1–C8**) had a good anti-PDAC potential.

Pancreatic ductal adenocarcinoma (PDAC) is one of the most common malignant tumors in the world with aggressive growth, high mortality and poor prognosis.[80,81] Chemotherapy is the main method for the treatment of first-line ductal carcinoma, but pancreatic cancer is diagnosed when it has already

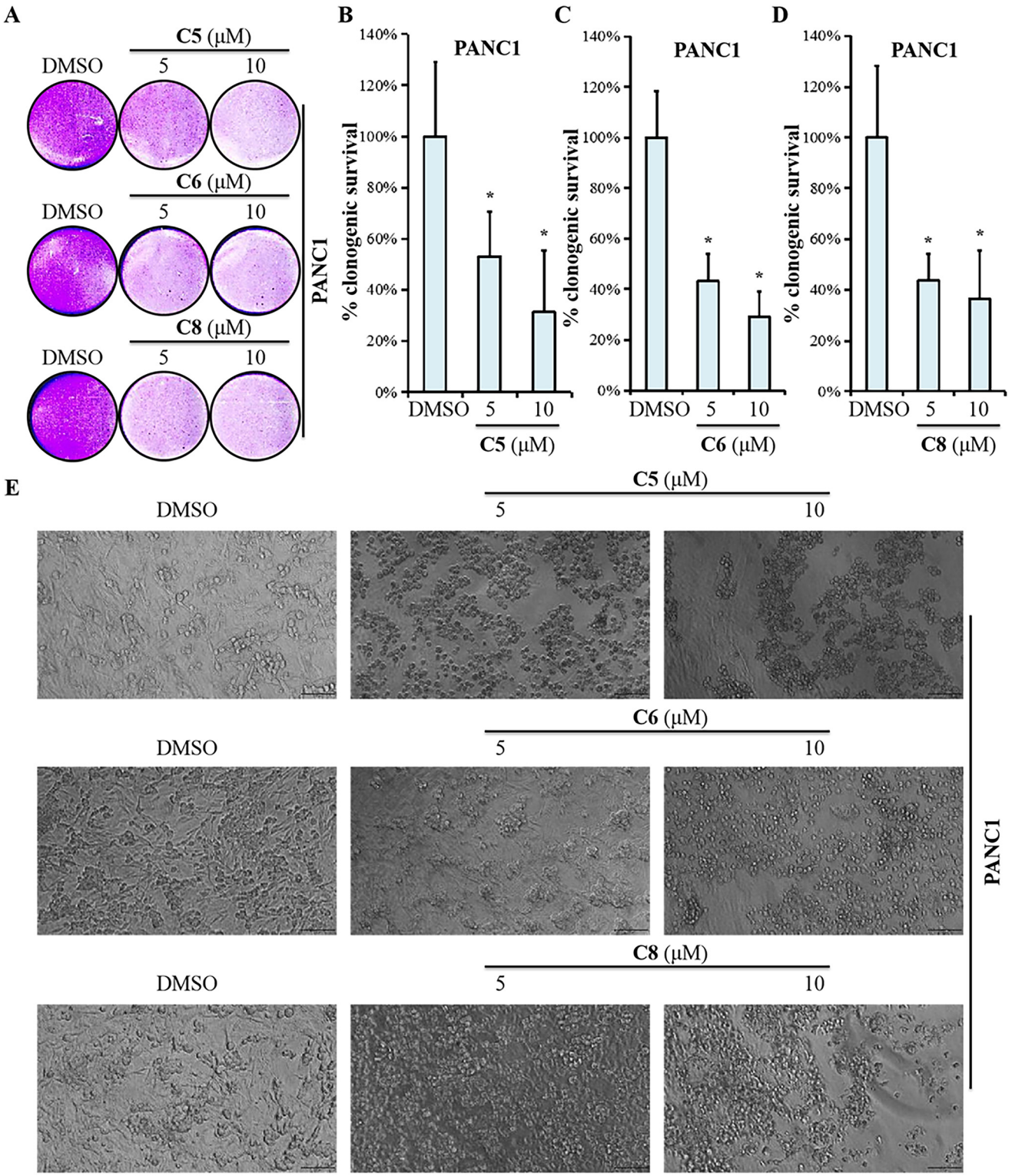

Fig. 12 Effect on clonogenic potential of PANC1 cells; (A–D) PANC1 cells were treated with DMSO, and 5 and 10 μM of **C5**, **C6** or **C8** for 7 days and clonogenic potential was determined using crystal violet staining assay. Color intensity reflected cell viability. (E) Morphological changes in PANC1 cells treated with DMSO, **C5**, **C6** or **C8** in a dose-dependent manner. Statistical analysis represents the student *t*-test; *$p < 0.05$; **$p < 0.005$.

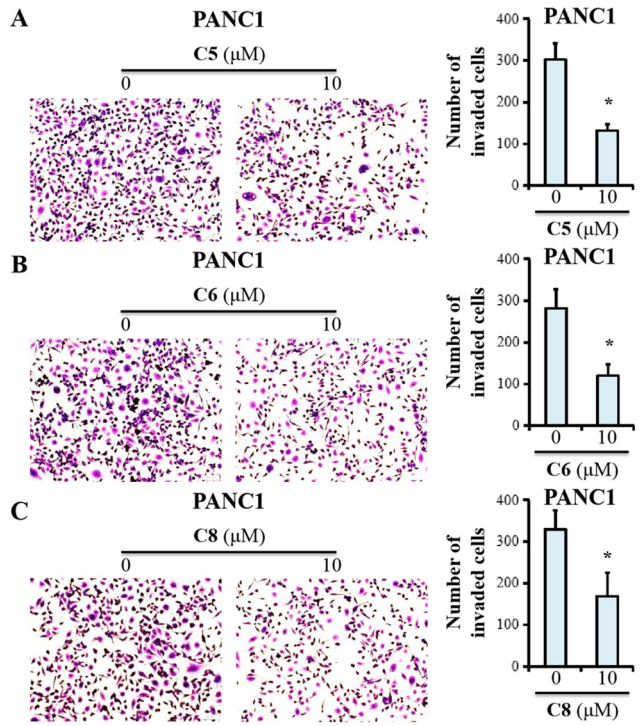

Fig. 13 Invasion of pancreatic cancer cells; (A–C) PANC1 cells were treated with DMSO or 10 μM of **C5**, **C6** or **C8** for 48 h, and invasion ability was determined using cell invasion assay. Data represent the number of invaded cells. Statistical analysis represents the student *t*-test; **p* < 0.05; ***p* < 0.005.

developed to the advanced stage, which has greatly reduced the therapeutic effect of existing chemotherapeutic drugs. Therefore, to cope with pancreatic cancer, it is necessary to develop more effective chemotherapeutic drugs.[82,83] In this scenario, the *in vitro* antitumor activity of the current series of these salicylaldehyde-derived piperazine functionalized hydrazone ligand-based platinum complexes (**C1–C8**) was studied. First, the cytotoxicity effect of **C1–C8** on three PDAC cell lines (BxPC3, MIAPaCa-2 and PANC1 cells) was determined by MTT assay. The results showed that **C1–C8** had certain cytotoxicity, among which **C5**, **C6** and **C8** exhibited the best comprehensive performance on these three cancer cells. We evaluated the dose-dependent cytotoxicity of **C5**, **C6** and **C8**, which showed a significant correlation. The key complexes among **C1–C8**, **C5**, **C6** and **C8** exhibited good cytotoxicity and anti-proliferative activity. Next, we compared the cytotoxicity of **C5**, **C6** and **C8** with commercially available chemotherapeutic drugs CP, 5-FU, OXA and DOX on BxPC3, MIAPaCa-2 and PANC1 cells. The cytotoxicity of **C5**, **C6** and **C8** was significantly stronger than these commercially available drugs. Furthermore, the effects of **C5**, **C6** and **C8** on the colony formation potential and invasion of PANC1 cells were determined. The results showed that these complexes inhibited the colony formation and invasion of tumor cells at a low concentration of 5 μM, thereby inhibiting the progression, metastasis and drug resistance of tumor cells. Simultaneously, when **C5**, **C6** and **C8** were combined with classic PARP inhibitors olaparib, veliparib and niraparib, the survival rate of PANC1 cells was significantly reduced. The combination of **C5**, **C6** and **C8** with olaparib, veliparib and niraparib showed superior synergistic antitumor activity, indicating that these three complexes are potential candidates for anti-PDAC. ATP, PARP and caspase3/7 are closely related to cancer cell apoptosis. Based on the above results, we selected **C5** to study these anti-PDAC mechanisms. PNAC1 cells were treated with **C5** in combination with olaparib, veliparib and niraparib, respectively. The results showed that **C5** had synergistic mechanisms with these anticancer drugs that caused DNA damage and inhibited the expression of PARP for DNA damage repair, which led to serious DNA damage, promoted the expression of pro-apoptotic factor caspase3/7, and triggered cancer cell apoptosis. However, PARP, as a substrate of caspase3/7, cleaved caspase3/7 and further reduced the expression of PARP. PARP repair of DNA damage requires stimulation to produce more ATP for energy because the expression of PARP is double inhibited, so there is no need to produce more ATP. It was confirmed that the combination of **C5** with olaparib, veliparib and niraparib inhibited the expression of PARP, promoted the expression of caspase3/7, reduced the production of ATP, comprehensively induced cancer cell apoptosis and exerted synergistic anti-PANC1 activity. Methylated histone transferase EZH2, which is closely related to tumorigenesis, invasion and metastasis, promotes cell cycle progression and self-renewal of tumor cells by inhibiting genes that lead to cell cycle arrest. The expression level of the EZH2 protein in PANC1 cells treated with **C5**, **C6** and **C8** was determined by western blot. It was found that the expression of the EZH2 protein was significantly inhibited, and the expression level of the EZH2 protein was significantly decreased. It was proved that **C5**, **C6** and **C8** inhibited the proliferation, invasion and metastasis of PANC1 cells by inhibiting the expression of EZH2 protein and thus inhibiting the cycle progression of PANC1 cells.

It was concluded that these piperazine-functionalized hydrazone ligand-based platinum complexes had anti-PDAC activity. Among them, **C5**, **C6** and **C8** exhibited the best antitumor activity. In PNAC1 cells, these complexes exerted synergistic antitumor effects when combined with PARP inhibitors olaparib, veliparib and niraparib. The combination of **C5** and these drugs induced the apoptosis of PNAC1 cells by inhibiting PARP expression, promoting caspase3/7 expression, and reducing ATP production. In addition, **C5**, **C6** and **C8** inhibited the proliferation, invasion and metastasis of PANC1 cells by inhibiting the expression of EZH2 protein. These results prove that these platinum complexes have potential as anti-PDAC drugs, which provides a basis for further detailed *in vitro* or *in vivo* biological investigation.

Materials and methods

Chemistry

General experimental and materials. All solvents and reagents were purchased from commercial sources. The ^{1}H and ^{13}C NMR spectroscopic analyses were conducted at 298 K using a Bruker AVANCE 500 MHz spectrometer. A Waters G2-Xs

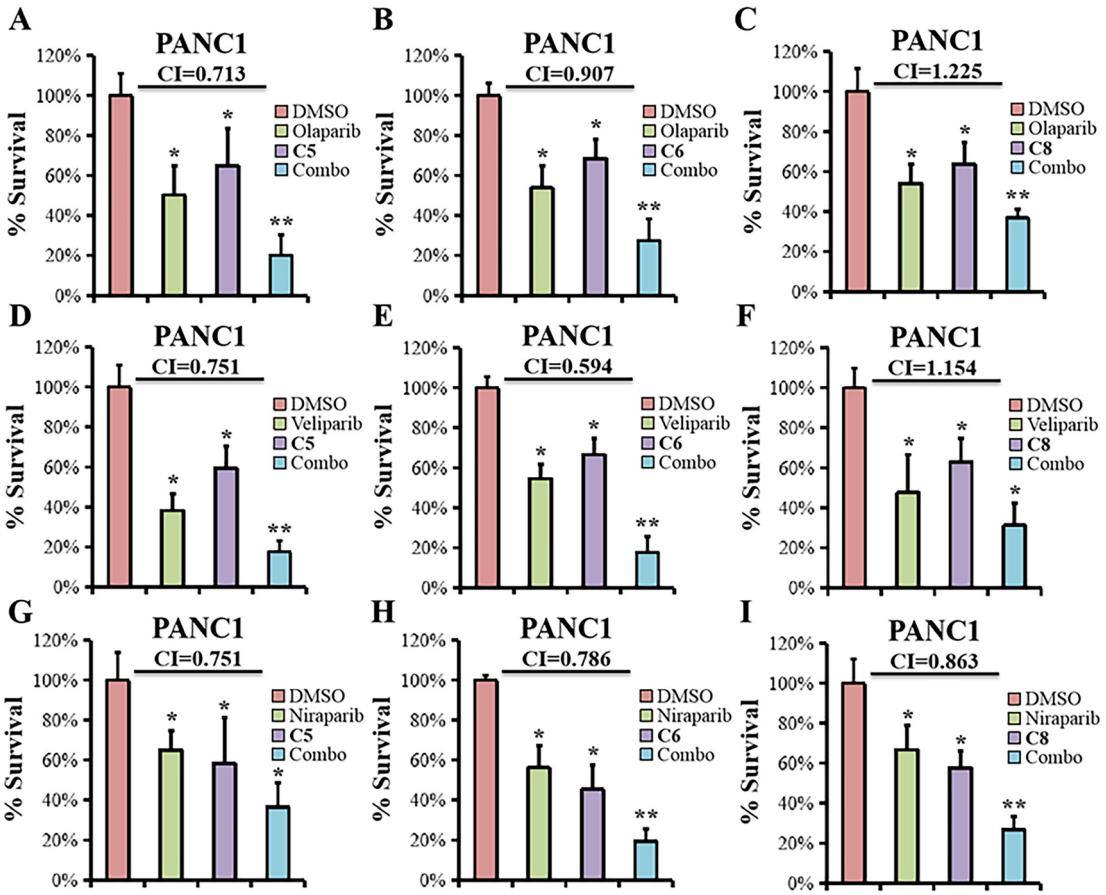

Fig. 14 Combined anticancer effect of **C5**, **C6** and **C8** with PARP inhibitors; (A–I) PANC1 cells were treated with DMSO; 10 μM of **C5**, **C6** and **C8**; 5 μM olaparib; 10 μM veliparib and 10 μM niraparib independently or in combination for 48 h, and cell viability was determined *via* MTT assay. Statistical analysis represents the student *t*-test; $*p < 0.05$; $**p < 0.005$.

QTof mass spectrometer was used for the HR-ESI-MS tests, and each compound CH_2Cl_2 solution was used in the mass analyses. X-ray single-crystal structure analyses were performed on a Rigaku Oxford Diffraction Supernova Dual Source, Cu at zero equipped with an AtlasS2 CCD using Cu Kα radiation. The data were collected and processed using the Oxford Diffraction, Xcalibur CCD System, CrysAlisPro (Oxford Diffraction Ltd: Abingdon, England, UK, 201024). The structures were solved by applying the direct method using Olex2 software,[84] and the non-hydrogen atoms were located from the trial structure and then refined anisotropically with SHELXL-2018[85] using a full-matrix least squares procedure based on F^2. The weighted R factor, wR and goodness-of-fit S values were obtained based on F^2. The hydrogen atom positions were fixed geometrically at the calculated distances and allowed to ride on their parent atoms. Crystallographic data of **C1**, **C5**, **C6**, **C7** and **C8** were submitted to Cambridge Crystallographic Data Center.

General procedure for the synthesis of L1–L8. 1 mmol of 1-amino-4-methylpiperazine was taken in 10 mL of ethanol in a 25 mL round bottom flask, and 1.2 mmol (1.2 equivalents) of particular salicylaldehyde was added to it. The resulting reaction mixture was stirred at reflux until completion (5 h) (checked by TLC, 1% MeOH/CH_2Cl_2 was used as eluent). After completion, it was cooled in a refrigerator for 6 h, which precipitated a white solid that was filtered and further washed with cold ethanol. The white solid recovered was dried in the air to a stable mass and characterized.

L1, 78% yield, white solid; FT-IR (KBr pellet) cm^{-1}: 3728.3, 3429.4, 1743.6, 1687.7, 1643.3, 1608.6, 1525.7, 1462.0, 1309.7, 1093.6, 750.3, 677.0. ^{1}H NMR (500 MHz, chloroform-*d*) δ 11.59 (s, 1H), 7.67 (s, 1H), 7.20–7.11 (m, 2H), 6.92 (d, J = 8.2 Hz, 1H), 6.85 (td, J = 7.5, 1.1 Hz, 1H), 3.20–3.15 (m, 4H), 2.64–2.59 (m, 4H), 2.35 (s, 3H) ppm. ^{13}C NMR (125 MHz, chloroform-*d*) δ 157.6, 140.6, 129.6, 119.0, 116.6, 54.1, 51.1, 45.9 ppm. HRMS (ESI): calculated for $C_{12}H_{18}N_3O$, 220.1450; found: 220.1451, $[M + H]^+$.

L2, 80% yield, white solid; FT-IR (KBr pellet) cm^{-1}: 3429.5, 2920.2, 1606.7, 1533.4, 1471.7, 1301.9, 1224.8, 1166.9, 1097.5, 1026.1, 952.8, 823.6, 738.7, 678.9. ^{1}H NMR (500 MHz, chloroform-*d*) δ 11.36 (s, 1H), 7.64 (s, 1H), 6.98 (dd, J = 8.3, 1.9 Hz, 1H), 6.93 (d, J = 1.8 Hz, 1H), 6.83 (d, J = 8.3 Hz, 1H), 3.18–3.15 (m, 4H), 2.63–2.59 (m, 4H), 2.35 (s, 3H), 2.26 (s, 3H) ppm. ^{13}C NMR (125 MHz, chloroform-*d*) δ 155.4, 140.8, 130.3, 129.9, 128.0, 118.7, 116.3, 54.1, 51.1, 45.9, 20.4 ppm. HRMS (ESI): calculated for $C_{13}H_{20}N_3O$, 234.1606; found: 234.1609, $[M + H]^+$.

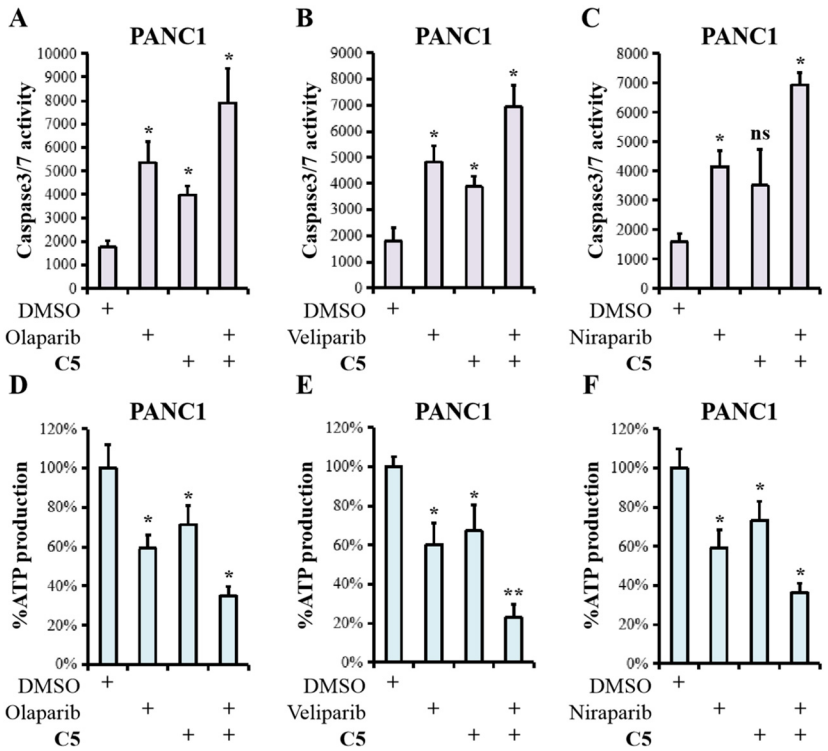

Fig. 15 **C5** in combination with PARP inhibitors induced apoptosis and reduced ATP production; (A–C) PANC1 cells were treated with DMSO, 10 μM of **C5**, 5 μM olaparib, 10 μM veliparib and 10 μM niraparib independently or in combination for 48 h, and caspase3/7activity was determined using a caspase3/7 activity kit; (D–F) PANC1 cells were treated with DMSO, 10 μM of **C5**, 5 μM olaparib, 10 μM veliparib and 10 μM niraparib independently or in combination for 48 h, and %ATP production was determined using an ATP determination kit. Statistical analysis represents the student *t*-test; **p* < 0.05; ***p* < 0.005; ns = non-specific.

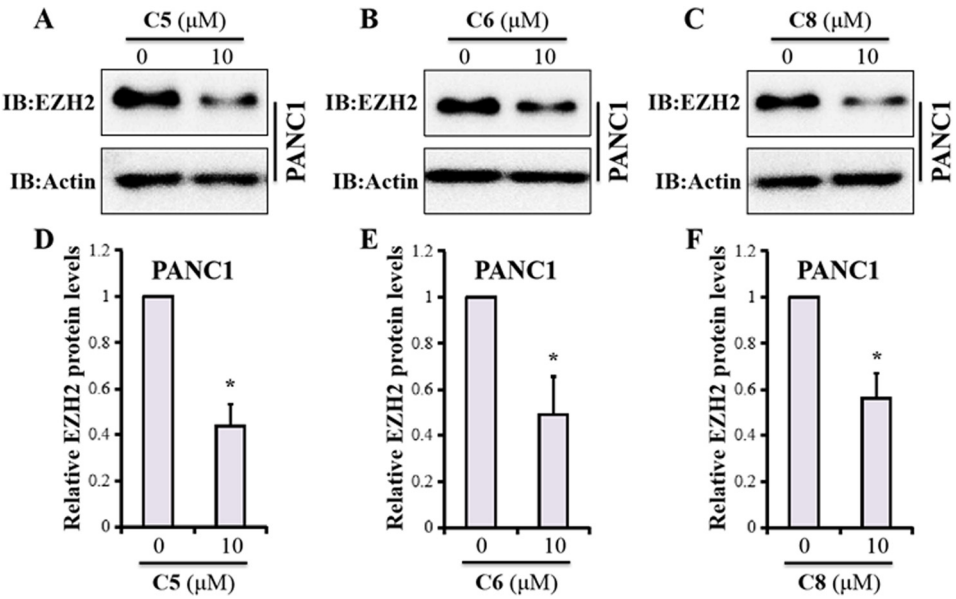

Fig. 16 Inhibition of EZH2 protein expression in pancreatic cancer cells; (A–C) PANC1 cells were treated with **C5**, **C6** or **C8** (10 μM) for 2 days, and EZH2 protein expression was determined *via* western blot. Actin was used as a loading control. (D–F) Data represent changes in EZH2 protein expression upon treatment with **C5**, **C6** or **C8** in PANC1 cells. Statistical analysis represents the student *t*-test **p* < 0.05.

L3, 83% yield, white solid; FT-IR (KBr pellet) cm^{-1}: 3417.8, 2912.5, 1604.8, 1521.8, 1450.5, 1408.0, 1301.9, 1172.7, 1126.4, 1089.8, 991.4, 947.0, 842.9, 798.5, 742.6, 684.7. ^{1}H NMR (500 MHz, chloroform-*d*) δ 11.11 (s, 1H), 7.61 (s, 1H), 6.85 (d, J = 8.9 Hz, 1H), 6.77 (dd, J = 8.9, 3.0 Hz, 1H), 6.67 (d, J = 3.0 Hz, 1H), 3.75 (s, 3H), 3.19–3.16 (m, 4H), 2.62–2.59 (m, 4H), 2.35 (s, 3H) ppm. ^{13}C NMR (125 MHz, chloroform-*d*) δ 152.4, 151.7, 140.1, 119.0, 117.1, 115.7, 114.1, 55.9, 54.1, 51.0, 45.9 ppm. HRMS (ESI): calculated for $C_{13}H_{20}N_3O_2$, 250.1556; found: 250.1558, $[M + H]^+$.

L4, 93% yield, white solid; FT-IR (KBr pellet) cm^{-1}: 3425.5, 2916.3, 1610.5, 1537.2, 1442.7, 1338.6, 1249.9, 1188.1, 1097.5, 1053.1, 1004.9, 952.8, 900.7, 827.5, 752.2. ^{1}H NMR (500 MHz, chloroform-*d*) δ 12.90 (s, 1H), 8.59 (s, 1H), 8.01 (d, J = 8.5 Hz, 1H), 7.76 (d, J = 7.8 Hz, 1H), 7.70 (d, J = 8.9 Hz, 1H), 7.48 (ddd, J = 8.4, 6.9, 1.3 Hz, 1H), 7.36–7.29 (m, 1H), 7.19 (d, J = 8.9 Hz, 1H), 3.33–3.22 (m, 4H), 2.72–2.62 (m, 4H), 2.38 (s, 3H) ppm. ^{13}C NMR (125 MHz, chloroform-*d*) δ 157.5, 137.8, 131.8, 130.9, 129.1, 128.2, 126.9, 123.0, 119.9, 119.2, 109.2, 54.2, 51.5, 45.9 ppm. HRMS (ESI): calculated for $C_{16}H_{20}N_3O$, 270.1606; found: 270.1612, $[M + H]^+$.

L5, 84% yield, white solid; FT-IR (KBr pellet) cm^{-1}: 3408.2, 2902.8, 1606.7, 1533.4, 1469.7, 1300.0, 1224.8, 1166.9, 1095.6, 1028.0, 954.8, 823.6. ^{1}H NMR (500 MHz, chloroform-*d*) δ 11.56 (s, 1H), 7.54 (s, 1H), 7.24 (dq, J = 4.5, 2.4 Hz, 2H), 6.82–6.79 (m, 1H), 3.20–3.17 (m, 4H), 2.62–2.59 (m, 4H), 2.35 (s, 3H) ppm. ^{13}C NMR (125 MHz, chloroform-*d*) δ 156.6, 138.3, 131.9, 131.6, 120.9, 118.4, 110.6, 54.0, 50.8, 45.9 ppm. HRMS (ESI): calculated for $C_{12}H_{17}N_3OBr$, 298.0555; found: 298.0554, $[M + H]^+$.

L6, 82% yield, white solid; FT-IR (KBr pellet) cm^{-1}: 3402.4, 2893.2, 1604.8, 1521.8, 1456.2, 1408.0, 1301.9, 1174.6, 1132.2, 1091.7, 945.1, 841.0, 796.6, 740.7, 667.4. ^{1}H NMR (500 MHz, chloroform-*d*) δ 11.53 (s, 1H), 7.54 (s, 1H), 7.12–7.07 (m, 2H), 6.85 (d, J = 8.8 Hz, 1H), 3.20–3.16 (m, 4H), 2.62–2.59 (m, 4H), 2.35 (s, 3H) ppm. ^{13}C NMR (125 MHz, chloroform-*d*) δ 156.1, 138.4, 129.0, 128.7, 123.6, 120.2, 117.9, 54.0, 50.8, 45.9 ppm. HRMS (ESI): calculated for $C_{12}H_{17}N_3OCl$, 254.1060; found: 254.1064, $[M + H]^+$.

L7, 80% yield, white solid; FT-IR (KBr pellet) cm^{-1}: 3398.5, 2879.68, 2856.53, 2358.9, 1608.6, 1533.4, 1460.1, 1421.5, 1300.0, 1207.4, 1145.7, 1099.4, 999.1, 958.6, 852.5, 817.8. ^{1}H NMR (500 MHz, chloroform-*d*) δ 11.32 (s, 1H), 7.55 (s, 1H), 7.06–6.63 (m, 3H), 3.21–3.16 (m, 4H), 2.61 (d, J = 10.3 Hz, 4H), 2.35 (s, 3H) ppm. ^{13}C NMR (125 MHz, chloroform-*d*) δ 156.8, 154.9, 153.6, 138.6, 119.3, 119.3, 117.4, 117.3, 116.0, 115.8, 115.0, 114.8, 54.1, 50.8, 45.9 ppm. HRMS (ESI): calculated for $C_{12}H_{17}N_3OF$, 238.1356; found: 238.1360, $[M + H]^+$.

L8, 90% yield, white solid; FT-IR (KBr pellet) cm^{-1}: 3404.3, 2914.4, 2358.9, 1604.8, 1548.8, 1483.2, 1464.0, 1440.8, 1319.3, 1193.9, 1093.6, 1022.3, 950.9, 898.8, 842.9, 792.7, 742.6, 665.4. ^{1}H NMR (500 MHz, chloroform-*d*) δ 12.48 (s, 1H), 8.10–8.03 (m, 2H), 7.63 (s, 1H), 6.96 (d, J = 9.0 Hz, 1H), 3.23 (d, J = 5.1 Hz, 4H), 2.64–2.61 (m, 4H), 2.36 (s, 3H) ppm. ^{13}C NMR (125 MHz, chloroform-*d*) δ 163.0, 140.3, 137.0, 125.2, 124.9, 119.0, 117.1, 53.9, 50.6, 45.9 ppm. HRMS (ESI): calculated for $C_{12}H_{17}N_3O_3$, 265.1301; found: 265.1304, $[M + H]^+$.

General procedure for the synthesis of C1–C8. 46 mg (0.11 mmol, 0.11 equivalent) of K_2PtCl_4 was taken in 1 mL of DMSO and heated at 50 °C with constant agitation to dissolve, which resulted in a reddish solution. 9 mg (0.11 equivalent) of NaOAc and 0.1 mmol (1 equivalent) of each ligand (**L1–L8**) were weighed together and added to the K_2PtCl_4 solution at 50 °C. The mixture was then added with 20 mL of MeOH at constant stirring, and the temperature was increased to reflux. It was stirred at this temperature until completion (checked by TLC until the ligand spot disappeared) (6 h). The mixture was cooled in a refrigerator for 6 h, and the formed light-yellow solid precipitate was filtered and washed with cold methanol. A pure product (**C1–C8**) was recovered in good isolated yield and characterized.

C1, 63% yield, light yellow solid; FT-IR (KBr pellet) cm^{-1}: 2937.5, 2810.2, 1598.6, 1599.0, 1491.0, 1452.4, 1406.1, 1278.8, 1205.5, 1151.5, 1084.0, 995.3, 943.2, 898.8, 788.9, 748.4, 677.0. ^{1}H NMR (500 MHz, DMSO-d_6) δ 8.97 (s, 1H), 7.50 (dd, J = 8.0, 1.8 Hz, 1H), 7.39 (ddd, J = 8.7, 6.9, 1.9 Hz, 1H), 6.74 (dd, J = 8.6, 1.0 Hz, 1H), 6.58 (ddd, J = 8.0, 6.8, 1.1 Hz, 1H), 3.54–3.40 (m, 2H), 3.31–3.23 (m, 4H), 2.77 (s, 3H), 2.60 (ddd, J = 11.3, 9.3, 6.1 Hz, 2H) ppm. ^{13}C NMR (125 MHz, DMSO-d_6) δ 162.8, 152.7, 134.5, 134.3, 121.0, 117.4, 116.1, 56.6, 52.3, 50.3 ppm. HRMS (ESI): calculated for $C_{12}H_{16}N_3OClPtNa$, 471.0527; found: 471.0522, $[M + Na]^+$.

C2, 69% yield, light yellow solid; FT-IR (KBr pellet) cm^{-1}: 2941.4, 2814.1, 1606.7, 1492.9, 1448.5, 1377.2, 1276.9, 1109.1, 995.3, 925.8, 827.5, 767.7, 682.8. ^{1}H NMR (500 MHz, DMSO-d_6) δ 8.88 (s, 1H), 7.30–7.25 (m, 1H), 7.22 (dd, J = 8.7, 2.3 Hz, 1H), 6.66 (d, J = 8.7 Hz, 1H), 3.48 (dq, J = 11.9, 6.1 Hz, 2H), 3.29–3.23 (m, 4H), 2.76 (s, 3H), 2.65–2.55 (m, 2H), 2.18 (s, 3H) ppm. ^{13}C NMR (125 MHz, DMSO-d_6) δ 161.2, 152.4, 136.1, 133.0, 124.3, 120.8, 116.7, 56.6, 52.3, 50.4, 20.0 ppm. HRMS (ESI): calculated for $C_{13}H_{18}N_3OClPtNa$, 485.0684; found: 485.0683, $[M + Na]^+$.

C3, 72% yield, light yellow solid; FT-IR (KBr pellet) cm^{-1}: 2941.4, 2837.2, 2798.7, 1612.6, 1489.0, 1444.7, 1375.2, 1259.5, 1211.3, 1155.3, 1001.0, 908.5, 829.4, 769.6, 678.9. ^{1}H NMR (500 MHz, DMSO-d_6) δ 8.93 (s, 1H), 7.09 (dd, J = 9.2, 3.3 Hz, 1H), 7.04 (d, J = 3.2 Hz, 1H), 6.69 (d, J = 9.2 Hz, 1H), 3.66 (s, 3H), 3.50–3.43 (m, 2H), 3.29–3.27 (m, 2H), 2.76 (s, 3H), 2.64–2.55 (m, 2H), 2.50 (dt, J = 3.5, 1.7 Hz, 2H) ppm. ^{13}C NMR (125 MHz, DMSO-d_6) δ 158.3, 152.2, 149.8, 124.9, 121.9, 115.8, 113.7, 56.5, 56.0, 52.3, 50.4 ppm. HRMS (ESI): calculated for $C_{13}H_{18}N_3O_2ClPtNa$, 501.0633; found: 501.0633, $[M + Na]^+$.

C4, 74% yield, light yellow solid; FT-IR (KBr pellet) cm^{-1}: 3049.4, 2937.5, 2833.4, 2791.0, 2754.3, 2358.9, 1899.9, 1784.1, 1616.3, 1589.3, 1512.2, 1460.1, 1363.7, 1282.6, 1242.1, 1151.5, 1001.0, 945.1, 891.1, 812.0, 738.7, 667.4. ^{1}H NMR (500 MHz, DMSO-d_6) δ 9.65 (s, 1H), 8.10 (d, J = 8.5 Hz, 1H), 7.88 (d, J = 9.2 Hz, 1H), 7.76 (d, J = 9.1 Hz, 1H), 7.52 (t, J = 7.7 Hz, 1H), 7.27 (t, J = 7.8 Hz, 1H), 6.95 (d, J = 9.2 Hz, 1H), 3.57–3.47 (m, 2H), 3.40 (ddd, J = 14.3, 9.2, 6.3 Hz, 2H), 3.34 (d, J = 4.6 Hz, 1H), 3.29 (d, J = 4.6 Hz, 1H), 2.81 (s, 3H), 2.68–2.57 (m, 2H) ppm. ^{13}C NMR

(125 MHz, DMSO-d_6) δ 163.0, 146.6, 134.5, 133.5, 129.0, 128.0, 127.5, 124.2, 123.3, 120.8, 107.30, 56.5, 52.4, 50.6 ppm. HRMS (ESI): calculated for $C_{16}H_{18}N_3OClPtNa$, 521.0684; found: 521.0682, $[M + Na]^+$.

C5, 78% yield, light yellow solid; FT-IR (KBr pellet) cm^{-1}: 3049.4, 2937.5, 2833.39, 2791.0, 2754.3, 2690.7, 2358.9, 1899.9, 1753.3, 1616.3, 1589.3, 1512.2, 1460.1, 1363.7, 1282.6, 1242.1, 1151.5, 1001.0, 945.1, 91.1, 806.2, 738.7, 667.4. ^{1}H NMR (500 MHz, DMSO-d_6) δ 9.00 (s, 1H), 7.38 (dd, J = 9.6, 3.3 Hz, 1H), 7.30 (ddd, J = 9.3, 8.0, 3.4 Hz, 1H), 6.74 (dd, J = 9.4, 4.8 Hz, 1H), 3.53–3.42 (m, 2H), 3.31–3.24 (m, 4H), 2.77 (s, 3H), 2.60 (ddd, J = 15.1, 7.4, 4.3 Hz, 2H) ppm. ^{13}C NMR (125 MHz, DMSO-d_6) δ 161.7, 152.1, 136.5, 135.3, 123.5, 119.3, 106.4, 56.6, 52.2, 50.3 ppm. HRMS (ESI): calculated for $C_{12}H_{15}N_3OClPtBrNa$, 548.9632; found: 548.9638, $[M + Na]^+$.

C6, 75% yield, light yellow solid; FT-IR (KBr pellet) cm^{-1}: 2945.3, 2837.2, 2802.5, 2358.9, 1595.1, 1479.4, 1444.7, 1373.3, 1267.2, 1192.0, 1149.6, 1107.1, 993.3, 918.1, 827.5, 767.7, 705.9, 648.1. ^{1}H NMR (500 MHz, DMSO-d_6) δ 9.03 (s, 1H), 7.64 (d, J = 2.8 Hz, 1H), 7.38 (dd, J = 9.1, 2.9 Hz, 1H), 6.75 (d, J = 9.2 Hz, 1H), 3.54–3.41 (m, 2H), 3.30–3.24 (m, 4H), 2.76 (s, 3H), 2.60 (ddd, J = 15.3, 12.4, 6.5 Hz, 2H) ppm. ^{13}C NMR (125 MHz, DMSO-d_6) δ 161.4, 152.2, 133.9, 132.3, 123.1, 119.2, 118.4, 56.6, 52.2, 50.3 ppm. HRMS (ESI): calculated for $C_{12}H_{15}N_3OClPtClNa$, 505.0138; found: 505.0137, $[M + Na]^+$.

C7, 67% yield, light yellow solid; FT-IR (KBr pellet) cm^{-1}: 2945.3, 2837.2, 2804.5, 2360.8, 1595.1, 1492.9, 1444.7, 1373.3, 1263.4, 1149.6, 995.3, 918.1, 827.5, 767.7, 678.9. ^{1}H NMR (500 MHz, DMSO-d_6) δ 9.02 (s, 1H), 7.76 (d, J = 2.7 Hz, 1H), 7.47 (dd, J = 9.1, 2.7 Hz, 1H), 6.70 (d, J = 9.1 Hz, 1H), 3.53–3.43 (m, 2H), 3.31–3.21 (m, 4H), 2.76 (s, 3H), 2.59 (ddd, J = 11.3, 9.0, 6.3 Hz, 2H) ppm. ^{13}C NMR (125 MHz, DMSO-d_6) δ 159.6, 152.4, 152.1, 152.1, 122.9, 122.7, 122.4, 122.4, 117.0, 116.8, 116.26, 116.2, 56.6, 52.2, 50.3 ppm. HRMS (ESI): calculated for $C_{12}H_{15}N_3OClPtFNa$, 489.0433; found: 489.0432, $[M + Na]^+$.

C8, 73% yield, light yellow solid; FT-IR (KBr pellet) cm^{-1}: 3080.3, 2945.3, 2850.8, 2798.7, 2358.9, 1595.1, 1452.4, 1340.5, 1286.5, 1203.6, 1151.5, 1087.8, 1084.0, 995.3, 925.8, 852.5, 806.2, 702.1, 640.4. ^{1}H NMR (500 MHz, DMSO-d_6) δ 9.29 (s, 1H), 8.70 (d, J = 3.0 Hz, 1H), 8.19 (dd, J = 9.5, 3.0 Hz, 1H), 6.85 (d, J = 9.5 Hz, 1H), 3.57–3.44 (m, 2H), 3.36 (d, J = 8.8 Hz, 2H), 3.30 (d, J = 9.5 Hz, 2H), 2.78 (s, 3H), 2.66–2.55 (m, 2H) ppm. ^{13}C NMR (125 MHz, DMSO-d_6) δ 167.1, 153.4, 137.4, 132.5, 128.0, 122.2, 117.4, 56.7, 52.1, 50.2 ppm. HRMS (ESI): calculated for $C_{12}H_{15}N_4O_3PtFNa$, 516.0378; found: 516.0381, $[M + Na]^+$.

Biology

Cell culturing. BxPC3, MIAPaCa-2, and PANC1 pancreatic cancer cells were obtained from ATCC and maintained in DMEM (Gibco) supplemented with 10% FBS (Gibco) and 1% PEST (penicillin–streptomycin) (Merk Millipore). BxPC3, MIAPaCa-2, and PANC1 cells were grown using an incubator at 37 °C and 5% CO_2.

Cell proliferation assay. MTT assay was used to determine the cell viability of BxPC3, MIAPaCa-2 and PANC1 cells. BxPC3, MIAPaCa-2, and PANC1 cells were treated with the indicated concentrations of different Pt complexes for 48 h, followed by an MTT assay to determine the cell proliferation ability of these cells. MTT reagent (3-(4,5-dimethylthiazol-2-yl)-2,5-diphenyltetrazolium bromide) (Thermo Fisher Scientific) was added, and 96 well plate cells were incubated in an incubator at 37 °C and 5% CO_2 for 2 h. Media was removed from cells; then, 100 μL of DMSO was added to the control groups and Pt complex-treated groups to dissolve formazan crystals. Reading was recorded at 490 nm, and calculations were performed.

Bright field images. BxPC3, MIAPaCa-2 and PANC1 cells were treated with the indicated complexes for 48 h. After that, bright field images were taken to detect morphological changes in the control and drug-treated BxPC3, MIAPaCa-2, and PANC1 cells.

Clonogenic potential assay. BxPC3, MIAPaCa-2, and PANC1 cells were treated with DMSO, 5 or 10 μM of **C5**, **C6** and **C8** for 3 days. Drug containing media was removed from BxPC3, MIAPaCa-2, and PANC1 cell lines; then, fresh media was added to cells. BxPC3, MIAPaCa-2, and PANC1 cells were maintained in DMEM supplemented with 10% FBS and 1% PEST (penicillin–streptomycin). 7 days later, the media was removed from BxPC3, MIAPaCa-2, and PANC1 cells and washed with 1× PBS carefully. Fixation was performed with fixation solution having a combination of acetic acid/methanol 1 : 7 ratio for 20 min at rt. The fixed cells were then stained with 0.5% crystal violet solution (Sigma Aldrich) for 20 min at rt. To remove excess crystal violet staining, cell plates were washed with water, and plates were dried, scanned and analyzed for the results.

Crystal violet reading and absorbance. After following the procedure of crystal violet staining and scanning of plates, a solution of 50% ethanol and acetic acid (1 : 1) was added to each well to dissolve the crystal violet staining. After that, a reading at 570 nm was taken, and calculations were performed.

Caspase 3/7 activity. PANC1 cells were treated with DMSO and **C5**, olaparib, veliparib and niraparib alone or in combinations for 48 h, and caspase3/7 activity assay was performed to detect apoptosis using Caspase-Glo® 3/7 assay system (Promega) following the manufacturer's instructions.

ATP assay. PANC1 cells were treated with DMSO and **C5**, veliparib, olaparib, and niraparib independently or in combinations for 48 h; then, an ATP assay was performed to detect ATP production using an ATP assay kit (ab83355, Abcam) following instructions from the manufacturer.

Drug synergism study. PANC1 cells were treated with DMSO and **C5**, **C6**, **C8**, olaparib, veliparib and niraparib alone or in combinations for 48 h; then, MTT assay was performed to determine cell proliferation ability, and the combination index was calculated for each combination in PANC1 cells.

Invasion assay. An invasion assay was performed using transwell inserts from corning, pre-coated with matrigel (BD). PANC1 cells were plated in transwell inserts and treated with DMSO and **C5**, **C6** or **C8** for 48 h. 500 μL medium supplemented with 20% FBS was used to fill the lower part of the

chambers. After 48 h of incubation, penetrated PANC1 cells were fixed with methanol fixation solution for 30 min at rt. The fixed cells were then stained with a solution of crystal violet (0.5%) for 15 min at rt. After that, the chambers were removed from the crystal violet solution and washed carefully with water to remove excess crystal violet staining. The chambers were dried, and images were taken.

Western blot. PANC1 cells were treated with DMSO and the indicated complexes for 48 h, followed by western blot analysis. Cell pellets were collected from both control and complex treated cells and lysed in RIPA lysis buffer containing 0.1% SDS, 50 μM Tris (pH 8.0), 1.0% NP-40, 0.5% sodium deoxycholate and 120 μM sodium chloride in combination with protease inhibitor cocktail. Samples were kept on ice for 25 min to complete the cell lysis. Lysed samples were centrifuged for 15 min at 4 °C, and the supernatant was collected. After completion of the running, the samples were transferred to a PVDF membrane, and the transfer was performed. 5% non-fat dry milk in 1× TBST was used for blocking. 1 h blocking was performed at rt. After that, the membranes were incubated with EZH2 and actin primary antibodies overnight at 4 °C. Next day, the primary antibodies were removed; then, membranes were washed with 1× TBST 3 times. Membranes were incubated with secondary antibody for 90 min on a shaker at rt. The secondary antibody was removed from the membranes and washed 3 times with 1× TBST. After that, an ECL solution (Pierce™ ECL western blotting substrate) was added to the membranes to detect the signal. EZH2 (D2C9) XP® rabbit mAb #5246 (cell signaling technology) and β-actin antibody #4967 (cell signaling technology) were used.

Data availability

The data supporting this article have been included as part of the ESI.†

Conflicts of interest

There are no conflicts to declare.

Acknowledgements

The authors acknowledge the Inner Mongolia University China funding under the title Academic Backbone (no. 10000-21311201/092), Inner Mongolia Autonomous Region China funding no. 21300-5213122 and "JUN-MA" High-level Talents Program of Inner Mongolia University China (no. 21300-5195112, 21300-5205107).

References

1 T. Zhong, J. Yu, Y. Pan, N. Zhang, Y. Qi and Y. Huang, *Adv. Healthcare Mater.*, 2023, **12**, 2300253.
2 T. R. Panda, M. Manikandan, S. P. Vaidya, S. Chhatar, S. Sinha, M. Mehrotra, S. Chakraborty, S. Gadre, P. Duari, P. Ray and M. Patra, *Angew. Chem., Int. Ed.*, 2023, **62**, 202303958.
3 M. E. Graziotto, M. C. Akerfeldt, A. P. Gunn, K. Yang, M. V. Somerville, N. V. Coleman, B. R. Roberts, T. W. Hambley and E. J. New, *J. Inorg. Biochem.*, 2017, **117**, 328–334.
4 D. Wang, G. Zhu, X. Huang and S. J. Lippard, *Proc. Natl. Acad. Sci. U. S. A.*, 2010, **197**, 9584–9589.
5 Z. Chen, S. Zhang, J. Zhang and Z. Zhu, *New J. Chem.*, 2017, **41**, 6760–6768.
6 C. Andrepont, P. A. Marzilli, S. Pakhomova and L. G. Marzilli, *J. Inorg. Biochem.*, 2015, **153**, 219–230.
7 B. Wang, Z. Wang, F. Ai, W. K. Tang and G. Zhu, *J. Inorg. Biochem.*, 2015, **142**, 118–125.
8 T. C. Johnstone, J. J. Wilson and S. J. Lippard, *Inorg. Chem.*, 2013, **52**, 12234–12249.
9 I. B. Lozada, B. Huang, M. Stilgenbauer, T. Beach, Z. Qiu, Y. Zheng and D. E. Herbert, *Dalton Trans.*, 2020, **49**, 6557–6560.
10 F. Liu, J. Suryadi and U. Bierbach, *Chem. Res. Toxicol.*, 2015, **28**, 2170–2178.
11 Y. Guo, Y. He, S. Wu, S. Zhang, D. Song, Z. Zhu, Z. Guo and X. Wang, *Inorg. Chem.*, 2019, **58**, 13150–13160.
12 F. Qi, H. Yuan, Y. Chen, Y. Guo, S. Zhang, Z. Liu, W. He and Z. Guo, *J. Inorg. Biochem.*, 2021, **218**, 111394.
13 T. T. Tasso, T. M. Tsubone, M. S. Baptista, L. M. Mattiazzi, T. V. Acunha and B. A. Iglesias, *Dalton Trans.*, 2017, **46**, 11037–11045.
14 T. Chatzisideri, S. Thysiadis, S. Katsamakas, P. Dalezis, I. Sigala, T. Lazarides, E. Nikolakaki, D. Trafalis, O. A. Gederaas, M. Lindgren and V. Sarli, *Eur. J. Med. Chem.*, 2017, **141**, 221–231.
15 N. Muhammad, C. Tan, M. Kamran, J. Wang, N. Sadia, Z. Pan, L. Ji and Z. Mao, *Inorg. Chem. Front.*, 2020, **7**, 4010–4019.
16 Z. L. Zhang, R. Rong, X. L. Ren, L. W. Xu, W. J. Lian, X. Qiao and J. Y. Xu, *Inorg. Chem. Front.*, 2023, **10**, 4157–4174.
17 H. Kostrhunova, J. Malina, A. J. Pickard, J. Stepankova, M. Vojtiskova, J. Kasparkova, T. Muchova, M. L. Rohlfing, U. Bierbach and V. Brabec, *Mol. Pharmaceutics*, 2011, **8**, 1941–1954.
18 Y. Li, Z. Sun, Y. Cui, H. Zhang, S. Zhang, X. Wang, S. Liu and Q. Gao, *Bioorg. Chem.*, 2021, **107**, 104636.
19 S. Jin, Y. Guo, Z. Guo and X. Wang, *Pharmaceuticals*, 2021, **13**, 133.
20 F. U. Rahman, A. Ali, R. Guo, Y. C. Zhang, H. Wang, Z. T. Li and D. W. Zhang, *Dalton Trans.*, 2015, **44**, 2166–2175.
21 F. U. Rahman, A. Ali, R. Guo, W. K. Wang, H. Wang, Z. T. Li, Y. Lin and D. W. Zhang, *Dalton Trans.*, 2015, **44**, 9872–9880.
22 X. Bai, A. Ali, Z. Lv, N. Wang, X. Zhao, H. Hao, Y. Zhang and F. U. Rahman, *Eur. J. Med. Chem.*, 2021, **224**, 113689.
23 X. Bai, A. Ali, N. Wang, Z. Liu, Z. Lv, Z. Zhang, X. Zhao, H. Hao, Y. Zhang and F. U. Rahman, *Eur. J. Med. Chem.*, 2022, **227**, 113920.

24 H. Kargar, M. F. Mehrjardi and K. S. Munawar, *Coord. Chem. Rev.*, 2024, **501**, 215587.
25 A. A. S. E. Etrawy and F. F. Sherbiny, *J. Mol. Struct.*, 2021, **1232**, 129993.
26 F. S. Tokalı, H. Şenol, Ş. Bulut and E. H. Aldoğan, *J. Mol. Struct.*, 2023, **1282**, 135176.
27 I. A. A. Azziz, N. H. Amin, M. T. E. Saadi and H. M. A. Rahman, *J. Mol. Struct.*, 2023, **1274**, 134583.
28 A. M. Sayed, F. A. Taher, M. R. K. A. Samad, M. S. A. E. Gaby, K. E. Adl and N. M. Saleh, *Bioorg. Chem.*, 2021, **108**, 104669.
29 S. Tasneem, K. A. Sheikh, M. Naematullah, M. M. Alam, F. Khan, M. Garg, M. Amir, M. Akhter, S. Amin, A. Haque and M. Shaquiquzzaman, *Bioorg. Chem.*, 2022, **126**, 105885.
30 G. G. Loescher, A. Schoenhuber, C. Ciglenec, S. Eberl, G. Krupitza, R. M. Mader, S. S. Jadav, V. Jayaprakash, M. F. Szekeres, T. Szekeres and P. Saiko, *Food Chem. Toxicol.*, 2017, **108**, 53–62.
31 H. S. J. Sonawane, R. S. Kalhapure and T. Govender, *Eur. J. Pharm. Sci.*, 2017, **99**, 45–65.
32 G. Sahu, K. Sahu, S. A. Patra, D. Mohapatra, R. Khangar, S. Sengupta and R. Dinda, *ACS Appl. Bio Mater.*, 2023, **6**, 5360–5371.
33 S. B. Markovic, N. Maciejewska, M. Olszewski, A. Visnjevac, A. Puerta, J. M. Padron, I. Novakovic, S. Kojic, H. S. Fernandes, S. F. Sousa, S. Ramotowska, A. Chylewska, M. Makowski, T. R. Todorovic and N. R. Filipovic, *Eur. J. Med. Chem.*, 2022, **238**, 114449.
34 M. Shit, S. Halder, K. Manna, A. K. Karan, A. Samanta, N. B. Manik, S. Pal, K. Jana and C. Sinha, *ACS Appl. Polym. Mater.*, 2024, **6**, 2637–2648.
35 J. Yuan, J. Y. Song, H. H. Yang, H. R. Lan, A. P. Xing, K. H. Li, D. Zeng, Z. Q. Zhang and S. Y. Feng, *J. Mol. Struct.*, 2023, **1276**, 134724.
36 Y. Wu, L. Hou, J. Lan, F. Yang, G. Huang, W. Liu and Y. Gou, *J. Mol. Struct.*, 2023, **1279**, 134986.
37 M. K. M. Subarkhan, L. Ren, B. Xie, C. Chen, Y. Wang and H. Wang, *Eur. J. Med. Chem.*, 2019, **179**, 246–256.
38 F. U. Rahman, M. Z. Bhatti, A. Ali, H. Q. Duong, Y. Zhang, X. Ji, Y. Lin, H. Wang, Z. T. Li and D. W. Zhang, *Eur. J. Med. Chem.*, 2028, **157**, 1480–1490.
39 J. Qi, Y. Zheng, B. Li, L. Wei, J. Li, X. Xu, S. Zhao, X. Zheng and Y. Wang, *Eur. J. Med. Chem.*, 2022, **237**, 114415.
40 F. U. Rahman, M. Z. Bhatti, A. Ali, H. Q. Duong, Y. Zhang, B. Yang, S. Koppireddi, Y. Lin, H. Wang, Z. T. Li and D. W. Zhang, *Eur. J. Med. Chem.*, 2018, **143**, 1039–1052.
41 K. Ostrowska, *Saudi Pharm. J.*, 2020, **28**, 220–232.
42 K. Gettys, Z. Ye and M. Dai, *Synthesis*, 2017, **49**, 2589–2604.
43 M. Shaquiquzzaman, G. Verma, A. Marella, M. Akhter, W. Akhtar, M. F. Khan, S. Tasneem and M. M. Alam, *Eur. J. Med. Chem.*, 2015, **102**, 487–529.
44 X. Jiang, B. Huang, S. Rumrill, D. Pople, W. A. Zalloum, D. Kang, F. Zhao, X. Ji, Z. Gao, L. Hu, Z. Wang, M. Xie, E. De Clercq, F. X. Ruiz, E. Arnold, C. Pannecouque, X. Liu and P. Zhan, *Commun. Chem.*, 2023, **6**, 83.
45 P. S. Girase, S. Dhawan, V. Kumar, S. R. Shinde, M. B. Palkar and R. Karpoormath, *Eur. J. Med. Chem.*, 2021, **210**, 112967.
46 N. Chiaramonte, A. Angeli, S. Sgambellone, A. Bonardi, A. Nocentini, G. Bartolucci, L. Braconi, S. Dei, L. Lucarini, E. Teodori, P. Gratteri, B. Wunsch, C. T. Supuran and M. N. Romanelli, *Eur. J. Med. Chem.*, 2022, **228**, 114026.
47 R. Pal, M. J. Akhtar, K. Raj, S. Singh, P. Sharma, S. Kalra, P. A. Chawla and B. Kumar, *J. Mol. Struct.*, 2022, **1257**, 132587.
48 S. Dhillon, *Drugs*, 2020, **80**, 433–439.
49 S. Goher, W. S. Abdrabo, G. B. Veerakanellore and B. Elgendy, *Curr. Pharm. Des.*, 2024, **30**, 597–623.
50 J. Y. Yu, X. Q. Li and M. X. Wei, *Eur. J. Med. Chem.*, 2019, **169**, 21–28.
51 M. X. Wei, J. Y. Yu, X. X. Liu, X. Q. Li, M. W. Zhang, P. W. Yang and J. H. Yang, *Eur. J. Med. Chem.*, 2021, **215**, 113295.
52 M. X. Wei, Y. X. Zhou, M. Lin, J. Zhang and X. Sun, *Eur. J. Med. Chem.*, 2022, **241**, 114651.
53 O. Zaim, O. Doganlar, Z. B. Doganlar, H. Ozcan, M. M. Zreigh and K. Kurtdere, *Bioorg. Chem.*, 2022, **129**, 106209.
54 F. U. Rahman, A. Ali, I. U. Khan, H. Q. Duong, S. B. Yu, Y. J. Lin, H. Wang, Z. T. Li and D. W. Zhang, *Eur. J. Med. Chem.*, 2017, **131**, 263–274.
55 W. Park, A. Chawla and E. M. O'Reilly, *J. Am. Med. Assoc.*, 2021, **326**, 851–862.
56 H. M. Kolbeinsson, S. Chandana, G. P. Wright and M. Chung, *J. Invest. Surg.*, 2023, **36**, 2129884.
57 L. D. Wood, M. I. Canto, E. M. Jaffee and D. M. Simeone, *Gastroenterology*, 2022, **163**, 386–402.
58 S. Wang, Y. Zheng, F. Yang, L. Zhu, X. Q. Zhu, Z. F. Wang, X. L. Wu, C. H. Zhou, J. Y. Yan, B. Y. Hu, B. Kong, D. L. Fu, C. Bruns, Y. Zhao, L. X. Qin and Q. Z. Dong, *Signal Transduction Targeted Ther.*, 2021, **6**, 249.
59 T. Muniraj, P. A. Jamidar and H. R. Aslanian, *Disease-a-Month*, 2013, **59**, 368–402.
60 H. Li, H. Wang, Y. Cui, W. Jiang, H. Zhan, L. Feng, M. Gao, K. Zhao, L. Zhang, X. Xie, N. Zhao, Y. Li and P. Liu, *Hereditas*, 2023, **160**, 23.
61 R. Duan, W. Du and W. Guo, *J. Hematol. Oncol.*, 2020, **13**, 104.
62 L. Gan, Y. Yang, Q. Li, Y. Feng, T. Liu and W. Guo, *Biomarker Res.*, 2018, **6**, 10.
63 K. S. Yan, C. Y. Lin, T. W. Liao, C. M. Peng, S. C. Lee, Y. J. Liu, W. P. Chan and R. H. Chou, *Int. J. Mol. Sci.*, 2017, **18**, 1172.
64 N. Wang, A. Ali, Z. Liu, H. Chi, Z. Lv, X. Zhao, Z. Zhang, H. Hao, Y. Zhang and F. U. Rahman, *Eur. J. Med. Chem.*, 2023, **258**, 115536.
65 M. J. Hsieh, T. J. Chiu, Y. C. Lin, C. C. Weng, Y. T. Weng, C. C. Hsiao and K. H. Cheng, *Int. J. Mol. Sci.*, 2020, **21**, 4473.
66 D. Xue, X. Zhou and J. Qiu, *Biomed. Pharmacother.*, 2020, **131**, 110676.

67 S. W. Brady, J. A. McQuerry, Y. Qiao, S. R. Piccolo, G. Shrestha, D. F. Jenkins, R. M. Layer, B. S. Pedersen, R. H. Miller, A. Esch, S. R. Selitsky, J. S. Parker, L. A. Anderson, B. K. Dalley, R. E. Factor, C. B. Reddy, J. P. Boltax, D. Y. Li, P. J. Moos, J. W. Gray, L. M. Heiser, S. S. Buys, A. L. Cohen, W. E. Johnson, A. R. Quinlan, G. Marth, T. L. Werner and A. H. Bild, *Nat. Commun.*, 2017, **8**, 1231.
68 S. Poon and L. E. Ailles, *Cancers*, 2022, **14**, 926.
69 A. A. Gopal, B. Fernandez, J. Delano, R. Weissleder and J. M. Dubach, *Cell Chem. Biol.*, 2024, **31**, 1–10.
70 K. G. Essel and K. N. Moore, *Expert Rev. Anticancer Ther.*, 2018, **18**, 727–733.
71 M. Robert, J. S. Frenel, C. Gourmelon, A. Patsouris, P. Augereau and M. Campone, *Expert Opin. Invest. Drugs*, 2017, **26**, 751–759.
72 H. S. Han, B. K. Arun, B. Kaufman, H. Wildiers, M. Friedlander, J. P. Ayoub, S. L. Puhalla, B. A. Bach, M. G. Kundu, N. Khandelwal, D. Feng, S. Bhattacharya, D. Maag, C. K. Ratajczak and V. Dieras, *Ann. Oncol.*, 2022, **33**, 299–309.
73 M. S. Hossan, M. K. B. Break, T. D. Bradshaw, H. M. Collins, C. Wiart, T. J. Khoo and A. Alafnan, *Molecules*, 2021, **26**, 2166.
74 T. Yokoyama, E. C. Kohn, E. Brill and J. M. Lee, *Int. J. Clin. Oncol.*, 2017, **50**, 1064–1074.
75 Á. Lahiguera, P. Hyroššová, A. Figueras, D. Garzón, R. Moreno, V. Sotocerrato, I. McNeish, V. Serra, C. Lazaro, P. Barretina, J. Brunet, J. Menéndez, X. Matiasguiu, A. Vidal, A. Villanueva, B. T. Harding, H. Tanaka, S. Orsulic, A. Junza, O. Yanes, C. M. Pinedo, L. Palomero, M. À. Pujana, J. C. Perales and F. Viñals, *EMBO Mol. Med.*, 2020, **12**, e11217.
76 E. Ma, P. Chen, H. M. Wilkins, T. Wang, R. H. Swerdlow and Q. Chen, *Free Radical Biol. Med.*, 2017, **113**, 36–47.
77 J. Velez, B. Dale, K. S. Park, H. U. Kaniskan, X. Yu and J. Jin, *Eur. J. Med. Chem.*, 2024, **267**, 116154.
78 S. Makita and K. Tobinai, *Lancet Oncol.*, 2018, **19**, 586–587.
79 Z. Dai and Z. Wang, *Molecules*, 2020, **25**, 5167.
80 A. Bararia, S. Dey, S. Gulati, S. Ghatak, S. Ghosh, S. Banerjee and N. Sikdar, *Hepatobiliary Pancreatic Dis. Int.*, 2020, **19**, 205–217.
81 W. Cai, W. Bao, S. Chen, Y. Yang and Y. Li, *Cancer Cell Int.*, 2021, **21**, 698.
82 C. B. Westphalen, S. Kruger, M. Haas, V. Heinemann and S. Boeck, *Expert Opin. Drug Saf.*, 2016, **15**, 947–954.
83 N. H. Tran and T. B. Saab, *JAMA Netw. Open*, 2021, **4**, e2134458.
84 O. V. Dolomanov, L. J. Bourhis, R. J. Gildea, J. A. K. Howard and H. Puschmann, *J. Appl. Crystallogr.*, 2009, **42**, 339–341.
85 D. Kratzert, J. J. Holstein and I. Krossing, *J. Appl. Crystallogr.*, 2015, **48**, 933–938.